Performance Analysis of Distributed Space–Time Block Coding Schemes in Middleton Class-A Noise

Roberto Savoia and Francesco Verde, *Member, IEEE*

***Abstract*—A performance analysis of distributed space–time block coding (STBC) schemes involving multiple decode-and-forward relays is carried out in the case of Middleton class-A impulsive noise, which is one of the major sources of performance degradation in many wireless systems. The considered cooperative communication framework, according to which the signal transmitted by each relay is the product of an STBC matrix and a proper vector of length L, encompasses both centralized and decentralized protocols. Since an insightful theoretical analysis of the maximum-likelihood (ML) detector is very challenging in non-Gaussian environments, an ideal version of the ML detector, which is referred to as ideal ML (IML), is considered, along with the suboptimal minimum-distance (MD) detector. It is analytically proven that, with respect to Gaussian noise, the presence of impulsive noise does not affect the performance of both the IML and MD detectors in terms of *asymptotic* (i.e., when the transmit power is infinitely large) diversity order $R_{\max}$, which is equal to the minimum between L and the maximum number of cooperating nodes (relays plus source); in the case of the IML detector, the coding gain is also unaffected. Closed-form formulas involving the main parameters of noise and STBC highlight that the major effect of impulse noise on the performance of the IML and MD detectors concerns the *finite* signal-to-noise ratio (SNR) diversity order, which does not monotonously increase as the SNR rises; in the case of the MD detector, the coding gain is also affected by the impulsiveness of noise. In particular, it is shown that, in the case of complex orthogonal STBC, the adverse effect of impulse noise on the performance of the IML detector tends to completely disappear for sufficiently large values of $R_{\max}$, whereas increasing values of $R_{\max}$ emphasize the weakness of the MD detector against non-Gaussian noise. Finally, simulation results are provided for the ML, IML, and MD detectors to corroborate and supplement the results theoretically derived.**

***Index Terms*—Cooperative diversity, decode-and-forward (D&F) relaying, distributed space–time block coding (STBC), maximum-likelihood (ML) decoding, Middleton class-A (MCA) noise, minimum-distance decoding.**

I. Introduction

COOPERATIVE *diversity* [1]–[4] arising from the presence of terminals distributed in space, which may serve as relay stations for a given source–destination pair, offers significant robustness against the adverse effects of fading in wireless communications, thus yielding higher reliability and throughput than direct transmission. *Decode-and-forward (D&F)* and *amplify-and-forward (A&F)* relaying are popular cooperation protocols. In the former protocol, the relay node forwards the source symbols if it has correctly decoded the received data; in the latter protocol, the relay node simply scales the received signal and retransmits it to the destination. Early cooperative communication schemes employed a single relay [1]–[3]; subsequently, multiple relays were allowed to forward signals at the same time [4]. In this latter case, to benefit from cooperative diversity without a significant loss in spectral efficiency, the use of *space–time block coding (STBC)* among the relays was proposed in [5]–[14], which was originally designed for colocated antennas [15], [16]. STBC rules can be employed in a *distributed* manner by allowing each relay to transmit a linear combination of L columns of a conventional STBC matrix. The weights of the aforementioned linear combination can be optimally assigned to each relay by a central unit [5], i.e., in a *centralized* fashion, which requires extra signaling overhead. On the other hand, such weights can be chosen by the relays locally in a random way [6]–[14], i.e., in a *decentralized* manner. Decentralized techniques eliminate the requirement of space–time codeword assignment and reduce coordination among the source and the relays, thus leading to a reduction in signaling cost.

Design and analysis of distributed STBC (DSTBC) rules [5]–[14] focus on the classical additive white Gaussian noise (AWGN) model. However, together with multipath fading, impulsive (non-Gaussian) noise is the prevalent source of performance degradation in many wireless scenarios, such as indoor, urban, rural, industrial, medical, commercial, modern local, and personal area networks [17]–[20]. Recently, use of cooperative techniques has been also proposed in [21] and [22] for power line communications. A widely accepted impulse noise model is *Middleton Class A (MCA)* [23]–[25], which was derived bearing in mind the real physical mechanisms that generate disturbance in communication receivers, whose validity has been confirmed by many measurement campaigns. Other well-known models are Bernoulli–Gauss [26], which can be regarded as an approximation to the more fundamental MCA noise model in many practical scenarios, and the symmetric alpha stable distribution [27], which models multiple-access interference in a multiuser network when the interfering nodes are scattered according to a spatial Poisson point process.

The combined effects of fading and impulsive noise on the performance of multiple-input–multiple-output (MIMO) systems with colocated antennas were studied in [28] and [29] by using the MCA noise model and in [30] by considering the symmetric alpha stable distribution. More recently,

Manuscript received March 12, 2012; revised September 25, 2012 and December 7, 2012; accepted January 9, 2013. This work was supported in part by Italian National Projects "HABITAT" and "DRIVE IN^2." The review of this paper was coordinated by Dr. X. Dong.

The authors are with the Department of Electrical Engineering and Information Technology, University of Naples Federico II, Naples 80125, Italy (e-mail: roberto.savoia@unina.it; f.verde@unina.it).

Color versions of one or more of the figures in this paper are available online at http://ieeexplore.ieee.org.

Digital Object Identifier 10.1109/TVT.2013.2240396

performance and optimization of cooperative diversity systems in impulsive noise have been considered in [31]–[33]. Both the A&F diversity scheme considered in [31] and the D&F cooperative system studied in [32] do not employ DSTBC by assuming that the source and the relays use orthogonal channels, e.g., the source and the relays transmit in different time slots or different frequency bands, and maximum-ratio combining techniques are used at the destination to extract the source information from the received signals. Although DSTBC is employed across the relays in [33], performance analysis in the case of minimum-distance (MD) detection at the destination is targeted at A&F relaying, and it is based on the assumption that impulsive noise samples at the relays and the destination are temporally dependent during a transmission frame.

The aim of this paper is to study the effects of both fading and impulsive noise on cooperative links employing multiple D&F relays with DSTBC, by completing and extending the preliminary results in [34]. To this goal, we use the MCA noise model, and, as decoding structures at the destination, we consider the maximum-likelihood (ML) detector, its *ideal* version (IML), and the MD detector that is suboptimum in non-Gaussian noise.[1] Our analysis shows that the IML detector is able to satisfactorily counteract the impulsiveness of noise in the *asymptotic* signal-to-noise ratio (SNR) regime,[2] by achieving an asymptotic diversity order $R_{\max}$ that is equal to the minimum between L and the maximum number of cooperating nodes (relays plus source). However, due to the closed-form formula directly linking the *finite-SNR* performance to the main parameters of both impulse noise and STBC, we highlight that the IML detector pays a penalty in terms of diversity order for a wide range of SNR values of practical interest; in particular, we show that, in the case of complex orthogonal STBC, such a penalty becomes negligible for increasing values of $R_{\max}$. It is also demonstrated that, although it ensures the same asymptotic diversity order $R_{\max}$ of the IML detector, the performance of the simpler MD detector is adversely affected not only in terms of finite-SNR diversity order but also in terms of coding gain; specifically, we show that, in the case of complex orthogonal STBC, there is an increase in such a penalty as $R_{\max}$ grows.

This paper is organized as follows. In Section II, the cooperative protocol is described, and the detection process at the relays is analyzed by using the MCA noise model introduced in Section I-A. The asymptotic- and finite-SNR performances of the IML and MD detectors are derived in Sections III and IV, respectively. Monte Carlo simulation results, in terms of average bit-error-rate (ABER) and finite-SNR diversity order, are presented in Section V for the ML, IML, and MD detectors and compared with our analytical results. Finally, some conclusions are drawn in Section VI.

[1] An alternative suboptimal method for reducing the adverse effect of impulse noise is to precede the MD detector with memoryless nonlinearity [35]. In some contexts, such as multiuser detection [36] and multicarrier modulation [37], this strategy allows bridging much of the gap between the IML (or ML) and the MD detector, without substantial increase in complexity. A detailed study of the tradeoff between performance and complexity of such detectors in the DSTBC framework at hand is outside the scope of this paper.

[2] Our numerical results show that ML and IML detectors substantially exhibit the same performances.

A. Notations and Preliminaries

The fields of complex, real, and nonnegative integer numbers are denoted by $\mathbb{C}$, $\mathbb{R}$, and $\mathbb{N}$, respectively; matrices (vectors) are denoted in uppercase (lowercase) boldface letters (e.g., $\mathbf{A}$ or $\mathbf{a}$); the field of $m \times n$ complex (real or nonnegative integer) matrices is denoted by $\mathbb{C}^{m\times n}$ ($\mathbb{R}^{m\times n}$ or $\mathbb{N}^{m\times n}$), with $\mathbb{C}^m$ ($\mathbb{R}^m$ or $\mathbb{N}^m$) used as a shorthand for $\mathbb{C}^{m\times 1}$ ($\mathbb{R}^{m\times 1}$ or $\mathbb{N}^{m\times 1}$); superscripts $*$, T, H, and -1 denote the conjugate, the transpose, the conjugate transpose, and the inverse of a matrix, respectively; $|\mathcal{A}|$ represents the cardinality of the set $\mathcal{A}$; $\min(x, y)$ $[\max(x, y)]$ is the minimum (maximum) value between $x \in \mathbb{R}$ and $y \in \mathbb{R}$; $\mathbf{0}_m \in \mathbb{R}^m$, $\mathbf{1}_m \in \mathbb{R}^m$, $\mathbf{O}_{m\times n} \in \mathbb{R}^{m\times n}$, and $\mathbf{I}_m \in \mathbb{R}^{m\times m}$ denote the null vector, the vector whose entries are all equal to 1, the null matrix, and the identity matrix, respectively; $\{\mathbf{a}\}_i$ indicates the ith element of $\mathbf{a} \in \mathbb{C}^m$, with $i \in \{1, 2, \ldots, m\}$; $\mathrm{rank}(\boldsymbol{A})$ is the rank of $\mathbf{A} \in \mathbb{C}^{m\times n}$; $\det(\boldsymbol{A})$ and $\mathrm{trace}(\mathbf{A})$ denote the determinant and the trace of $\mathbf{A} \in \mathbb{C}^{n\times n}$, respectively; $\|\boldsymbol{a}\|$ is the Euclidean norm of $\boldsymbol{a} \in \mathbb{C}^n$; the eigenvalues of a matrix $\mathbf{A} \in \mathbb{C}^{m\times m}$ are denoted by $\mu_i(\mathbf{A})$, for $i \in \{1, 2, \ldots, m\}$, and, when they are real, they are ordered as $\mu_1(\mathbf{A}) \geq \mu_2(\mathbf{A}) \geq \cdots \geq \mu_m(\mathbf{A})$; let $\mathbf{A} \in \mathbb{C}^n$ and $\mathbf{B} \in \mathbb{C}^n$ be Hermitian matrices, we write $\mathbf{A} \succ \mathbf{B}$ $[\mathbf{A} \succeq \mathbf{B}]$ if the matrix $\mathbf{A} - \mathbf{B}$ is positive definite (semidefinite); $\binom{n}{k}$ is the binomial coefficient, for n, $k \in \mathbb{N}$; $o(x)$ denotes the Landau symbol, i.e., for a function $f(x) = o(g(x))$, the ratio $f(x)/g(x) \to 0$, as $x \to 0$; $\mathrm{Q}(x) \triangleq (1/\sqrt{2\pi}) \int_x^{+\infty} e^{-u^2/2}\, du$ denotes the Q function; $P(A)$ denotes the probability that an event A occurs, and $P(A|B)$ is the conditional probability of A given an event B; the operator $\mathrm{E}[\cdot]$ denotes ensemble averaging and, specifically, $\mathrm{E}_{\tilde{\mathbf{x}}|\tilde{\mathbf{Y}}}[\cdot]$ is the conditional mean with respect to the random vector $\tilde{\mathbf{x}} \in \mathbb{C}^m$ given the random matrix $\tilde{\mathbf{Y}} \in \mathbb{C}^{n\times k}$; if $\tilde{\mathbf{Y}} = \mathbf{Y}$, the value of the random variable (RV) $\mathrm{E}_{\tilde{\mathbf{x}}|\tilde{\mathbf{Y}}}[\cdot]$ is denoted by $\mathrm{E}_{\tilde{\mathbf{x}}|\tilde{\mathbf{Y}}=\mathbf{Y}}[\cdot]$; a circular symmetric complex Gaussian random vector $\boldsymbol{x} \in \mathbb{C}^n$ with mean $\boldsymbol{\mu} \in \mathbb{C}^n$ and covariance matrix $\boldsymbol{K} \in \mathbb{C}^{n\times n}$ is denoted by $\boldsymbol{x} \sim \mathcal{CN}(\boldsymbol{\mu}, \boldsymbol{K})$.

In the high-SNR regime, the average symbol error probability (ASEP) for a digital communication system over a fading channel usually behaves as $\mathrm{ASEP}(\gamma) \leq (G_c\gamma)^{-G_d}$ [38], where γ denotes the average SNR, G_c is the coding gain, and G_d is the *asymptotic* diversity order; at an arbitrary SNR γ, the *finite-SNR* diversity order $G_d(\gamma)$ is defined [39] by the negative slope of the log–log plot of the average pairwise error probability (APEP) versus SNR, i.e.,

$$G_d(\gamma) \triangleq -\frac{d\log\left[\mathrm{APEP}(\gamma)\right]}{d\log(\gamma)} = -\frac{\gamma}{\mathrm{APEP}(\gamma)}\frac{d\mathrm{APEP}(\gamma)}{d\gamma} \quad (1)$$

which converges to G_d for asymptotically high SNR values.

According to [23]–[25], the MCA complex noise RV $\tilde{x}$ is the sum of two independent components: a Gaussian component $\tilde{n}$ with variance $\sigma_{\tilde{n}}^2$ and an interfering component $\tilde{\imath}$ with variance $\sigma_{\tilde{\imath}}^2$, and its probability density function (pdf) $f_{\tilde{x}}(x)$, with $x \in \mathbb{C}$, is given by

$$f_{\tilde{x}}(x) = \sum_{m=0}^{+\infty} p_{\widetilde{m}}(m) f_{\tilde{x}|\widetilde{m}}(x|m) \quad (2)$$

with

$$f_{\tilde{x}|\widetilde{m}}(x|m) \triangleq \frac{1}{\pi\sigma^2\sigma_m^2}\exp\left\{-\frac{|x|^2}{\sigma^2\sigma_m^2}\right\} \quad (3)$$

$$p_{\widetilde{m}}(m) \triangleq \exp\{-\lambda\}\frac{\lambda^m}{m!} \quad \text{and} \quad \sigma_m^2 \triangleq \frac{m\lambda^{-1}+\Gamma}{1+\Gamma} \quad (4)$$

where λ is the impulsive index, i.e., the average number of impulses affecting the receiver in a symbol period; $\Gamma \triangleq \sigma_{\tilde{n}}^2/\sigma_{\tilde{i}}^2 > 0$ is the Gaussian-to-impulse ratio; and $\sigma^2 = \sigma_{\tilde{n}}^2 + \sigma_{\tilde{i}}^2$ is the variance of $\tilde{x}$. Such a model comes from the assumption that the number of interfering impulses affecting the receiver is a Poisson RV $\widetilde{m}$ with parameter λ, whose probability mass function (pmf) is denoted by $p_{\widetilde{m}}(m)$, which represents the probability of having $m \in \mathbb{N}$ impulses within the considered symbol period. It is seen from (2) that $f_{\tilde{x}|\widetilde{m}}(x|m)$ is the conditional pdf of $\tilde{x}$ given $\widetilde{m} = m$ and, thus, $\tilde{x}|\widetilde{m} \sim \mathcal{CN}(0, \sigma^2\sigma_m^2)$. The parameters λ and Γ control the "impulsiveness" of noise. For $\lambda \ll 1$, the noise $\tilde{x}$ becomes more and more impulsive; for $\lambda \geq 1$, the probability distribution of $\tilde{x}$ approaches that of Gaussian noise[3]; for small values of Γ, the noise becomes more impulsive; the noise tends to be Gaussian for large values of Γ.

II. Cooperative Transmission Scheme and Performance Analysis at the Relays

We consider a wireless network where $N_{\max}$ randomly and independently placed *potential* relay nodes might assist the data transmission between a given source–destination pair. Each node in the network employs a single transmit/receive antenna. The relays work in half-duplex mode, i.e., they cannot transmit and receive at the same time, and they adopt a D&F relaying protocol. The link between each node pair is modeled as a frequency-flat[4] Rayleigh block-fading channel, i.e., it is characterized by a single fading coefficient that remains constant within $P > 0$ symbol intervals. Let the source wish to send the block $\tilde{\mathbf{a}} \triangleq [\tilde{a}_1, \tilde{a}_2, \ldots, \tilde{a}_K]^T \in \mathbb{C}^K$ toward the destination, with $K \leq P$, which is composed of independent and identically distributed (i.i.d.) zero-mean unit-variance equiprobable symbols. The vector $\tilde{\mathbf{a}}$ assumes values in the *symbol set* $\mathcal{A} = \{\mathbf{a}_1, \mathbf{a}_2, \ldots, \mathbf{a}_{|\mathcal{A}|}\}$. Cooperative transmission takes place in two phases.

In Phase I (*broadcast phase*), which spans a time interval of K consecutive symbol periods, the source broadcasts the symbol vector $\tilde{\mathbf{a}}$ to all the potential relays, which try to decode it. The discrete-time baseband equivalent received signal at the nth relay is given by $\tilde{\mathbf{z}}_n = \tilde{f}_n\tilde{\mathbf{a}} + \tilde{\mathbf{w}}_n$, for $n \in \{1, 2, \ldots, N_{\max}\}$, where $\tilde{f}_n$ denotes the channel gain between the source and the nth relay, whereas the entries of the noise vector $\tilde{\mathbf{w}}_n \triangleq [\tilde{w}_{n,1}, \tilde{w}_{n,2}, \ldots, \tilde{w}_{n,K}]^T \in \mathbb{C}^K$ are modeled as i.i.d. MCA RVs [29], [40], whose pdf is given by (2), with parameters Γ, λ, and variance $\sigma^2 \triangleq \mathrm{E}[|\tilde{w}_{n,k}|^2]$. Moreover, according to the Rayleigh-fading assumption, the channel vector $\tilde{\mathbf{f}} \triangleq [\tilde{f}_1, \tilde{f}_2, \ldots, \tilde{f}_{N_{\max}}]^T \in \mathbb{C}^{N_{\max}}$ is modeled as $\tilde{\mathbf{f}} \sim \mathcal{CN}(\mathbf{0}_{N_{\max}}, \mathbf{\Sigma}_{\tilde{\mathbf{f}}})$, with $\mathbf{\Sigma}_{\tilde{\mathbf{f}}} \triangleq \mathrm{diag}(\sigma_{\tilde{f}_1}^2, \sigma_{\tilde{f}_2}^2, \ldots, \sigma_{\tilde{f}_{N_{\max}}}^2)$, which is independent of $\tilde{\mathbf{a}}$ and $\{\tilde{\mathbf{w}}_n\}_{n=1}^{N_{\max}}$. Assuming that error detection mechanisms such as cyclic redundancy check are employed at the potential relays, only those nodes that successfully decode $\tilde{\mathbf{a}}$ will serve as relays in the subsequent phase, whose number is unknown and randomly time varying. Following the related literature, e.g., [1], [5], and [6], perfect synchronization is assumed at the symbol level among the source and the relays.

In Phase II (*cooperative phase*), which spans a time interval of P consecutive symbol periods, all the *active* relays, along with the source, simultaneously transmit in the same frequency band a space–time block coded version of $\tilde{\mathbf{a}}$, and it is assumed that the destination uses only the data received in such a phase to decode the source symbols. More precisely, as done in standard STBC [15], [16], the source and each active relay first map the vector $\tilde{\mathbf{a}}$ onto a given STBC matrix $\boldsymbol{\mathcal{C}}(\tilde{\mathbf{a}}) \in \mathbb{C}^{P\times L}$, where $L \geq 2$ denotes the number of *virtual* antennas in the underlying space–time code. Without considering any specific code structure, we only assume that the code matrix satisfies the rank criterion [16], which states that for any pair $\boldsymbol{\mathcal{C}}_k \triangleq \boldsymbol{\mathcal{C}}(\mathbf{a}_k)$ and $\boldsymbol{\mathcal{C}}_\ell \triangleq \boldsymbol{\mathcal{C}}(\mathbf{a}_\ell)$, where $\mathbf{a}_k, \mathbf{a}_\ell \in \mathcal{A}$ with $k \neq \ell$, the matrix $\boldsymbol{\mathcal{C}}_{k,\ell} \triangleq \boldsymbol{\mathcal{C}}_k - \boldsymbol{\mathcal{C}}_\ell$ is full rank, i.e., $\mathrm{rank}(\boldsymbol{\mathcal{C}}_{k,\ell}) = \min(P, L)$. Then, the source and each active relay virtually act as a single antenna in a multiple-antenna transmitter, by transmitting a linear combination of the columns of $\boldsymbol{\mathcal{C}}(\tilde{\mathbf{a}})$. Specifically, let $\tilde{\mathbf{r}}_n \in \mathbb{C}^L$ be a *signature* vector containing the linear combination coefficients for the nth node, the transmitted code $\tilde{\mathbf{x}}_n \in \mathbb{C}^P$ is given by $\tilde{\mathbf{x}}_n = \boldsymbol{\mathcal{C}}(\tilde{\mathbf{a}})\tilde{\mathbf{r}}_n$, for $n \in \{0, 1, \ldots, N_{\max}\}$ (where $n = 0$ is the representative index of the source), and then, the baseband equivalent discrete-time signal received at the destination assumes the form

$$\begin{aligned}\tilde{\mathbf{y}} &= \tilde{g}_0\tilde{\mathbf{x}}_0 + \sum_{n=1}^{N_{\max}} \tilde{s}_n\tilde{g}_n\tilde{\mathbf{x}}_n + \tilde{\mathbf{d}} \\ &= \boldsymbol{\mathcal{C}}(\tilde{\mathbf{a}})\tilde{\boldsymbol{\mathcal{R}}}\tilde{\mathbf{S}}\tilde{\mathbf{g}} + \tilde{\mathbf{d}} = \boldsymbol{\mathcal{C}}(\tilde{\mathbf{a}})\tilde{\mathbf{h}} + \tilde{\mathbf{d}}\end{aligned} \quad (5)$$

where $\tilde{g}_0$ is the channel coefficient between the source and the destination; for $n \in \{1, 2, \ldots, N_{\max}\}$, $\tilde{s}_n \in \{0, 1\}$ is a binary RV indicating if the nth relay is active in Phase II (i.e., if it correctly decoded the symbols of $\tilde{\mathbf{a}}$), with $\tilde{s}_{n_1}$ statistically independent of $\tilde{s}_{n_2}$, for $n_1 \neq n_2 \in \{1, 2, \ldots, N_{\max}\}$; $\tilde{g}_n$ denotes the fading channel gain between the nth active relay and the destination; the matrix $\tilde{\boldsymbol{\mathcal{R}}} \triangleq [\tilde{\mathbf{r}}_0, \tilde{\mathbf{r}}_1, \ldots, \tilde{\mathbf{r}}_{N_{\max}}] \in \mathbb{C}^{L\times(N_{\max}+1)}$ collects the signature vectors used by the source and the relays; according to the Rayleigh-fading assumption, the vector $\tilde{\mathbf{g}} \triangleq [\tilde{g}_0, \tilde{g}_1, \ldots, \tilde{g}_{N_{\max}}]^T \in \mathbb{C}^{N_{\max}+1}$ is modeled as $\tilde{\mathbf{g}} \sim \mathcal{CN}(\mathbf{0}_{N_{\max}+1}, \mathbf{\Sigma}_{\tilde{\mathbf{g}}})$, with $\mathbf{\Sigma}_{\tilde{\mathbf{g}}} \triangleq \mathrm{diag}(\sigma_{\tilde{g}_0}^2, \sigma_{\tilde{g}_1}^2, \ldots, \sigma_{\tilde{g}_{N_{\max}}}^2)$, which is statistically independent of $\tilde{\mathbf{S}} \triangleq \mathrm{diag}(1, \tilde{s}_1, \tilde{s}_2, \ldots, \tilde{s}_{N_{\max}}) \in \mathbb{R}^{(N_{\max}+1)\times(N_{\max}+1)}$; the vector $\tilde{\mathbf{h}} \triangleq \tilde{\boldsymbol{\mathcal{R}}}\tilde{\mathbf{S}}\tilde{\mathbf{g}} \in \mathbb{C}^L$ represents the *overall* channel between the cooperating nodes in Phase II and the destination; the vector $\tilde{\mathbf{d}} \triangleq [\tilde{d}_1, \tilde{d}_2, \ldots,$

[3] In the case of $\lambda = 10$, the noise $\tilde{x}$ can be regarded as a circular symmetric complex Gaussian RV.

[4] This assumption is made for the sake of simplicity and might be removed. If the channel is frequency selective, orthogonal frequency-division multiplexing techniques may be used to transform a frequency-selective channel into parallel frequency-nonselective channels.

$\tilde{d}_P]^T \in \mathbb{C}^P$ denotes additive noise, which is independent of $\tilde{\mathbf{a}}$ and $\tilde{\mathbf{h}}$, whose entries are modeled as i.i.d. MCA RVs [29], [40], whose pdf is given by (2), with parameters Γ, λ, and variance $\sigma^2 \triangleq \mathrm{E}[|\tilde{d}_p|^2]$.[5] The signal model (5) is quite general and subsumes different DSTBC approaches. In a *centralized* approach [1], each simultaneously transmitting node transmits a *preassigned* column of the STBC matrix $\boldsymbol{\mathcal{C}}(\tilde{\mathbf{a}})$, i.e., $L = N_{\max} + 1$, and $\tilde{\boldsymbol{\mathcal{R}}}$ is proportional to $\mathbf{I}_{N_{\max}+1}$. In a *decentralized deterministic* scheme [5], matrix $\tilde{\boldsymbol{\mathcal{R}}}$ has to be properly optimized. In the *decentralized randomized* coding rule developed in [6]–[14], the vector $\tilde{\mathbf{r}}_n$ is random and locally generated at the nth node. It is worth noting that in decentralized strategies, there is *no* relationship between L and the number of active relays in Phase II, and thus, L can be chosen without knowing what is the number of relays that are simultaneously transmitting.

With regard to the statistical characterization of the RVs $\tilde{s}_1, \tilde{s}_2, \ldots, \tilde{s}_{N_{\max}}$, it is seen [41] that $\tilde{s}_n$ is a Bernoulli RV, whose success probability is $P(\tilde{s}_n = 1) = (1 - \mathrm{ASEP}_n)^K$, for $n \in \{1, 2, \ldots, N_{\max}\}$, where ASEP_n is the *average* (over the random gain $\tilde{f}_n$) symbol error probability (SEP) at the output of the ML detector of the nth relay, which is modulation dependent. It can be shown [42] that, in the case of memoryless modulation schemes, the following result holds:

$$\mathrm{ASEP}_n = \sum_{m=0}^{+\infty} p_{\widetilde{m}}(m) \mathrm{ASEP}_{n,\mathrm{RAY}}\left(\sigma^2 \sigma_m^2\right) \tag{6}$$

where $\mathrm{ASEP}_{n,\mathrm{RAY}}(\sigma^2\sigma_m^2)$ is the average SEP (ASEP) for a Rayleigh-fading channel affected by AWGN with variance $\sigma^2\sigma_m^2$, which can be (approximatively) expressed [43] as

$$\mathrm{ASEP}_{n,\mathrm{RAY}}\left(\sigma^2\sigma_m^2\right) = \alpha\left(1 - \sqrt{\frac{\beta\sigma_{\tilde{f}_n}^2}{\sigma^2\sigma_m^2 + \beta\sigma_{\tilde{f}_n}^2}}\right) \tag{7}$$

with α and β being modulation-dependent parameters that depend on the constellation size. For instance, in the case of QPSK modulation, it results that $\alpha = 1$ and $\beta = 1/2$.

III. Performance Analysis of the Maximum-Likelihood Detector

The optimum detector makes a decision on $\tilde{\mathbf{a}}$ based on the observation of a particular realization $\mathbf{y}$ of the received vector $\tilde{\mathbf{y}}$ in (5) such that the probability of correct decision is maximized, provided that the noise pdf parameters λ, Γ, and σ^2 are exactly known.[6] Since $\tilde{\mathbf{a}}$ assumes values in $\mathcal{A}$ with equal probability, under the assumption that the realization $\mathbf{h}$ of the channel vector $\tilde{\mathbf{h}}$ is perfectly known by the destination,[7] optimum detection corresponds [43] to the ML criterion. Choose the vector $\mathbf{a}_k$ that maximizes the conditional pdf of $\tilde{\mathbf{y}}$ given that $\tilde{\mathbf{a}} = \mathbf{a}_k$ was transmitted and $\tilde{\mathbf{h}} = \mathbf{h}$, which is denoted by $f_{\tilde{\mathbf{y}}|\tilde{\mathbf{a}},\tilde{\mathbf{h}}}(\mathbf{y}|\mathbf{a}_k, \mathbf{h})$. Since $f_{\tilde{\mathbf{y}}|\tilde{\mathbf{a}},\tilde{\mathbf{h}}}(\mathbf{y}|\mathbf{a}_k, \mathbf{h}) = f_{\tilde{\mathbf{d}}}(\mathbf{y} - \boldsymbol{\mathcal{C}}_k\mathbf{h})$, one has the decision rule

$$\widehat{\mathbf{a}}_{\mathrm{ml}} = \arg \max_{k\in\{1,2,\ldots,|\mathcal{A}|\}} \prod_{p=1}^{P} \sum_{m_p=0}^{+\infty} \frac{p_{\widetilde{m}_p}(m_p)}{\pi\sigma^2\sigma_{m_p}^2} \cdot \exp\left\{-\frac{|\{\mathbf{y} - \boldsymbol{\mathcal{C}}_k\mathbf{h}\}_p|^2}{\sigma^2\sigma_{m_p}^2}\right\}. \tag{8}$$

For practical implementations, it is customary to resort to the *normalized* M-term truncation $\widehat{f}_{\tilde{d}_p}(d_p)$ of the pdf given in (2) (see [45] for details), which converges pointwise to $f_{\tilde{d}_p}(d_p)$ as $M \to +\infty$. Starting from $\widehat{f}_{\tilde{d}_p}(d_p)$, the infinite series in (8) is replaced with a sum having only M terms.

Performance measures of the ML decoder are $\mathrm{ASEP}_{\mathrm{ml}} \triangleq \mathrm{E}[\mathrm{SEP}_{\mathrm{ml}}(\tilde{\mathbf{h}})]$, where $\mathrm{SEP}_{\mathrm{ml}}(\tilde{\mathbf{h}})$ is the SEP at the output of the ML decoder [43], conditioned on $\tilde{\mathbf{h}}$, and $\mathrm{APEP}_{\mathrm{ml}} \triangleq \mathrm{E}[\mathrm{PEP}_{\mathrm{ml}}(\tilde{\mathbf{h}})]$, where $\mathrm{PEP}_{\mathrm{ml}}(\tilde{\mathbf{h}}) \triangleq P(\{\mathbf{a}_k \to \mathbf{a}_\ell\}_{\mathrm{ml}}|\tilde{\mathbf{h}})$ is the pairwise error probability (PEP) of the ML detector [6], conditioned on $\tilde{\mathbf{h}}$, i.e., the probability that $\mathbf{a}_\ell$ is detected at the destination when $\mathbf{a}_k$ was transmitted. Due to the awkward expression of the ML decision rule (8), exact computation of $\mathrm{ASEP}_{\mathrm{ml}}$ and $\mathrm{APEP}_{\mathrm{ml}}$ is very difficult, even when union bounding techniques are used. However, with reference to a MIMO system with colocated antennas, it has been numerically shown in [29] that the ASEP performance of the ML detector (8) is very similar to that of the *ideal* ML (IML) detector, which has perfect knowledge of the realization of $\widetilde{\mathbf{m}} \triangleq [\widetilde{m}_1, \widetilde{m}_2, \ldots, \widetilde{m}_P]^T \in \mathbb{N}^P$.[8] For the distributed framework at hand, this behavior is confirmed by the simulation results in Section V. Let $\boldsymbol{\Sigma}_{\mathbf{m}} \triangleq \mathrm{diag}(\sigma_{m_1}^2, \sigma_{m_2}^2, \ldots, \sigma_{m_P}^2) \in \mathbb{R}^{P\times P}$, the IML criterion amounts to choosing the vector $\mathbf{a}_k$ that maximizes the conditional pdf of $\boldsymbol{\Sigma}_{\mathbf{m}}^{-1/2}\tilde{\mathbf{y}}$ given that $\tilde{\mathbf{a}} = \mathbf{a}_k$ was transmitted, $\tilde{\mathbf{h}} = \mathbf{h}$ was acquired, and $\widetilde{\mathbf{m}} = \mathbf{m} \triangleq [m_1, m_2, \ldots, m_P] \in \mathbb{N}^P$. Since $\boldsymbol{\Sigma}_{\mathbf{m}}^{-1/2}\tilde{\mathbf{d}} \sim \mathcal{CN}(\mathbf{0}_P, \sigma^2\mathbf{I}_P)$, the IML decision rule ends up to

$$\widehat{\mathbf{a}}_{\mathrm{iml}} = \arg \min_{k\in\{1,2,\ldots,|\mathcal{A}|\}} (\mathbf{y} - \boldsymbol{\mathcal{C}}_k\mathbf{h})^H \boldsymbol{\Sigma}_{\boldsymbol{m}}^{-1} (\mathbf{y} - \boldsymbol{\mathcal{C}}_k\mathbf{h}) \tag{9}$$

whose PEP is simpler to analyze than that of (8). Let $\mathrm{PEP}_{\mathrm{iml}}(\tilde{\mathbf{h}}, \widetilde{\mathbf{m}}) \triangleq P(\{\mathbf{a}_k \to \mathbf{a}_\ell\}_{\mathrm{iml}}|\tilde{\mathbf{h}}, \widetilde{\mathbf{m}})$ be the PEP, conditioned on $\tilde{\mathbf{h}}$ and $\widetilde{\mathbf{m}}$, at the output of the IML decoder, it can be analytically shown that $\mathrm{PEP}_{\mathrm{iml}}(\mathbf{h}, \mathbf{m}) \le \mathrm{PEP}_{\mathrm{ml}}(\mathbf{h})$ for $\tilde{\mathbf{h}} = \mathbf{h}$ and $\widetilde{\mathbf{m}} = \mathbf{m}$, which is the consequence of the fact that, with respect to the ML case, the IML detector utilizes the additional knowledge of $\widetilde{\mathbf{m}} = \mathbf{m}$. As previously announced, our simulation results show that $\mathrm{APEP}_{\mathrm{iml}} \triangleq \mathrm{E}[\mathrm{PEP}_{\mathrm{iml}}(\tilde{\mathbf{h}}, \widetilde{\mathbf{m}})]$ turns out to be an approximation of $\mathrm{APEP}_{\mathrm{ml}}$ and not necessarily a lower bound.

[5] We have assumed for the sake of simplicity that the noise variances at the relays and at the destination are all equal.

[6] The expectation–maximization algorithm can be used [44] to derive estimates for the parameters of the MCA noise model.

[7] The relevant channel vector realization $\mathbf{h}$ can be estimated at the destination by allowing each data transmission in Phase II to be preceded by a training period, wherein all the active relays transmit a symbol sequence known to the destination; the signature vectors used during the training phase will be maintained in the subsequent data transmission.

[8] Such a detector is ideal since knowledge or estimation of a particular realization of $\widetilde{\mathbf{m}}$ is unrealistic, and for such a reason, it has been referred to as the genie-aided detector in [29].

From (9), the PEP at the output of the IML decoder is given by

$$\begin{aligned}\mathrm{PEP}_{\mathrm{iml}}(\mathbf{h},\mathbf{m}) &= \mathrm{Q}\left(\frac{\left\|\boldsymbol{\Sigma}_{\mathbf{m}}^{-1/2}\boldsymbol{\mathcal{C}}_{k,\ell}\mathbf{h}\right\|}{\sqrt{2\sigma^2}}\right)\\ &= \frac{1}{\pi}\int_0^{\pi/2}\exp\left(-\frac{\mathbf{h}^H\boldsymbol{\mathcal{C}}_{k,\ell}^H\boldsymbol{\Sigma}_{\mathbf{m}}^{-1}\boldsymbol{\mathcal{C}}_{k,\ell}\mathbf{h}}{4\sigma^2\sin^2\theta}\right)d\theta \quad (10)\end{aligned}$$

where the last equality is the consequence of a change in variables from rectangular to polar coordinates in the integral defining the Q-function. Recalling that $\tilde{\mathbf{h}} = \tilde{\boldsymbol{\mathcal{R}}}\tilde{\mathbf{S}}\tilde{\mathbf{g}}$, we keep the signature matrix $\tilde{\boldsymbol{\mathcal{R}}}$ fixed, i.e., $\tilde{\boldsymbol{\mathcal{R}}} = \boldsymbol{\mathcal{R}}$, with $\boldsymbol{\mathcal{R}} \in \mathbb{C}^{L\times(N_{\max}+1)}$ being a certain matrix with $R_{\max} \triangleq \mathrm{rank}(\boldsymbol{\mathcal{R}}) = \min(L, N_{\max}+1)$, and we average $\mathrm{PEP}_{\mathrm{iml}}(\tilde{\mathbf{h}},\tilde{\mathbf{m}})$ over all the realizations of $\tilde{\mathbf{s}} \triangleq [\tilde{s}_1, \tilde{s}_2, \ldots, \tilde{s}_{N_{\max}}]^T \in \mathbb{R}^{N_{\max}}$ (which collects the random diagonal entries of $\tilde{\mathbf{S}}$), $\tilde{\mathbf{g}}$, and $\tilde{\mathbf{m}}$.

In the sequel, we first study the performance of the IML detector in the high-SNR regime by evaluating the asymptotic diversity order, and then, we focus on its achievable finite-SNR diversity order.

A. Analysis of the IML Detector in the High-SNR Region

Let $\mathbf{S} \triangleq \mathrm{diag}(1, s_1, s_2, \ldots, s_{N_{\max}}) \in \mathbb{R}^{(N_{\max}+1)\times(N_{\max}+1)}$ be a realization of the matrix $\tilde{\mathbf{S}}$, with $\sum_{n=1}^{N_{\max}} s_n = N(\mathbf{s})$, where the vector $\mathbf{s} \triangleq [s_1, s_2, \ldots, s_{N_{\max}}]^T \in \mathbb{R}^{N_{\max}}$ is the corresponding realization of $\tilde{\mathbf{s}}$, i.e., only $N(\mathbf{s}) \le N_{\max}$ relays are active in Phase II, for sufficiently high (but finite) SNR values, the ASEP at the output of the IML detector, given $\tilde{\boldsymbol{\mathcal{R}}} = \boldsymbol{\mathcal{R}}$ and $\tilde{\mathbf{s}} = \mathbf{s}$, can be approximated (see, e.g., [43]) as in (11) shown at the bottom of the page, where N_e is the average number of minimum-distance neighbors for $\mathcal{A}$.

The following theorem holds:

Theorem 1 (IML ASEP for a Fixed Number of Active Relays): Let us assume, without loss of generality, that $P \ge L$ and the diagonal entries of $\boldsymbol{\Sigma}_{\tilde{\mathbf{g}}}$ are arranged in increasing order, i.e., $\sigma^2_{\tilde{g}_0} \le \sigma^2_{\tilde{g}_1} \le \cdots \le \sigma^2_{\tilde{g}_N}$, and define the average SNR as $\gamma \triangleq 1/\sigma^2$. It results that

$$\mathrm{ASEP}_{\mathrm{iml}}(\boldsymbol{\mathcal{R}},\mathbf{s}) \lessapprox \Upsilon(N(\mathbf{s}))\left[\prod_{r=1}^{R(\mathbf{s})}\frac{1}{\mu_r(\mathbf{S}\boldsymbol{\mathcal{R}}^H\boldsymbol{\mathcal{R}}\mathbf{S})}\right]\gamma^{-R(\mathbf{s})} \quad (12)$$

where $R(\mathbf{s}) \triangleq \mathrm{rank}(\boldsymbol{\mathcal{R}}\mathbf{S}) = \min(L, N(\mathbf{s})+1)$ and

$$\begin{aligned}\Upsilon\left(N(\mathbf{s})\right) \triangleq N_e\Theta &\left[\prod_{r=N(\mathbf{s})-R(\mathbf{s})+1}^{N(\mathbf{s})}\frac{1}{\sigma^2_{\tilde{g}_r}}\right]\\ &\cdot\left[\max_{\substack{k,\ell\in\{1,2,\ldots,|\mathcal{A}|\}\\ \ell\neq k}}\prod_{r=L-R(\mathbf{s})+1}^{L}\frac{1}{\mu_r(\boldsymbol{\mathcal{C}}_{k,\ell}^H\boldsymbol{\mathcal{C}}_{k,\ell})}\right] \quad (13)\end{aligned}$$

with $\Theta \triangleq (4^{R(\mathbf{s})}/\pi)\int_0^{\pi/2}(\sin^2\theta)^{R(\mathbf{s})}d\theta$.

Proof: See Appendix A. ■

Theorem 1 shows that the impact of MCA noise on the high-SNR performance of the IML (or ML) detector is similar to that of the Gaussian noise considered in [6]. Strictly speaking, the IML detector is able to completely counteract the "impulsiveness" of noise in the high-SNR regime.

Equation (12) characterizes the performance of the IML detector for a given realization $\mathbf{s}$ of the vector $\tilde{\mathbf{s}}$, which means that the number of active relays is fixed to the value $N(\mathbf{s})$. To take into account randomness in the number of active relays, the next step is to further average (12) with respect to $\tilde{\mathbf{s}}$, thus obtaining $\mathrm{ASEP}_{\mathrm{iml}}(\boldsymbol{\mathcal{R}}) \triangleq \mathrm{E}_{\tilde{\mathbf{s}}|\tilde{\boldsymbol{\mathcal{R}}}=\boldsymbol{\mathcal{R}}}[\mathrm{ASEP}_{\mathrm{iml}}(\tilde{\boldsymbol{\mathcal{R}}},\tilde{\mathbf{s}})]$. Accounting for the statistical characterization of $\tilde{\mathbf{s}}$ discussed in Section II, one has

$$\begin{aligned}\mathrm{ASEP}_{\mathrm{iml}}(\boldsymbol{\mathcal{R}}) = \sum_{\mathbf{s}\in\{0,1\}^{N_{\max}}}&\left\{\prod_{n=1}^{N_{\max}}[P(\tilde{s}_n=1)]^{s_n}\right.\\ &\left.\cdot[1-P(\tilde{s}_n=1)]^{1-s_n}\right\}\mathrm{ASEP}_{\mathrm{iml}}(\boldsymbol{\mathcal{R}},\mathbf{s}) \quad (14)\end{aligned}$$

where we recall that $P(\tilde{s}_n=1) = (1-\mathrm{ASEP}_n)^K$, with ASEP_n given by (6) and (7). To obtain an approximation of $\mathrm{ASEP}_{\mathrm{iml}}(\boldsymbol{\mathcal{R}})$ valid in the high-SNR regime, we observe that if $\sigma^2\sigma^2_m \ll \beta\sigma^2_{\tilde{f}_n}$, which is equivalent to $\gamma \gg \sigma^2_m/(\beta\sigma^2_{\tilde{f}_n})$, then (7) can be approximated [38] as $\mathrm{ASEP}_{n,\mathrm{RAY}}(\sigma^2\sigma^2_m) \approx (\alpha\sigma^2_m)/(2\beta\gamma\sigma^2_{\tilde{f}_n})$, for any[9] finite values of m. Hence, it follows from (4) and (6) that

$$\mathrm{ASEP}_n \approx \frac{\alpha}{2\beta\gamma\sigma^2_{\tilde{f}_n}}\frac{\mathrm{E}[\tilde{m}]\lambda^{-1}+\Gamma}{1+\Gamma} = \frac{\alpha}{2\beta\gamma\sigma^2_{\tilde{f}_n}} \quad (15)$$

where we have also used the fact that $\mathrm{E}[\tilde{m}] = \lambda$. Furthermore, at a high SNR, it holds that $(1-\mathrm{ASEP}_n)^K \approx 1-K\mathrm{ASEP}_n \approx 1$ and $1-(1-\mathrm{ASEP}_n)^K \approx K\mathrm{ASEP}_n$. Consequently, also owing to (12), the following upper bound on (14) can be written in the high-SNR region:

$$\begin{aligned}\mathrm{ASEP}_{\mathrm{iml}}(\boldsymbol{\mathcal{R}}) &\lessapprox \sum_{\mathbf{s}\in\{0,1\}^{N_{\max}}}\left\{\prod_{n=1}^{N_{\max}}\left[\frac{\alpha K}{2\beta\sigma^2_{\tilde{f}_n}}\right]^{1-s_n}\right\}\Upsilon\left(N(\mathbf{s})\right)\\ &\quad\cdot\left[\prod_{r=1}^{R(\mathbf{s})}\frac{1}{\mu_r(\mathbf{S}\boldsymbol{\mathcal{R}}^H\boldsymbol{\mathcal{R}}\mathbf{S})}\right]\gamma^{-[R(\mathbf{s})+N_{\max}-N(\mathbf{s})]}\\ &= \sum_{n=0}^{N_{\max}}\mathrm{ASEP}_{\mathrm{iml}}^{(n)}(\boldsymbol{\mathcal{R}})\gamma^{-[\min(L,n+1)+N_{\max}-n]} \quad (16)\end{aligned}$$

where

$$\begin{aligned}\mathrm{ASEP}_{\mathrm{iml}}^{(n)}(\boldsymbol{\mathcal{R}}) \triangleq \Upsilon(n)&\left(\frac{\alpha K}{2\beta\sigma^2_{\tilde{f}_n}}\right)^{N_{\max}-n}\\ &\cdot\sum_{\substack{\mathbf{s}\in\{0,1\}^{N_{\max}}\\ \text{with } N(\mathbf{s})=n}}\left[\prod_{r=1}^{R(\mathbf{s})}\frac{1}{\mu_r(\mathbf{S}\boldsymbol{\mathcal{R}}^H\boldsymbol{\mathcal{R}}\mathbf{S})}\right]. \quad (17)\end{aligned}$$

[9] If λ is small, the first few terms of the infinite sum in (6) dominate the value of ASEP_n.

$$\mathrm{ASEP}_{\mathrm{iml}}(\boldsymbol{\mathcal{R}},\mathbf{s}) \approx N_e\cdot\max_{\substack{k,\ell\in\{1,2,\ldots,|\mathcal{A}|\}\\ \ell\neq k}}\mathrm{E}_{\tilde{\mathbf{m}}|\tilde{\mathbf{s}}=\mathbf{s},\tilde{\boldsymbol{\mathcal{R}}}=\boldsymbol{\mathcal{R}}}\left\{\mathrm{E}_{\tilde{\mathbf{g}}|\tilde{\mathbf{m}},\tilde{\mathbf{s}}=\mathbf{s},\tilde{\boldsymbol{\mathcal{R}}}=\boldsymbol{\mathcal{R}}}\left[\mathrm{PEP}_{\mathrm{iml}}(\tilde{\mathbf{h}},\tilde{\mathbf{m}})\right]\right\} \quad (11)$$

The upper bound in (16) is expressed as a power sum in the average SNR γ, where the nth coefficient $\mathrm{ASEP}_{\mathrm{iml}}^{(n)}(\boldsymbol{\mathcal{R}})$ collects all the other relevant parameters for the $\binom{N_{\max}}{n}$ different network configurations with n active relays. Specifically, when $L \geq N_{\max}+1$, one has that $R_{\max} = N_{\max}+1$; hence, it follows from (16) that $\min(L, n+1) + N_{\max} - n = N_{\max}+1$, for each $n \in \{0, 1, \ldots, N_{\max}\}$, thus obtaining

$$\mathrm{ASEP}_{\mathrm{iml}}(\boldsymbol{\mathcal{R}}) \lessapprox \left[\sum_{n=0}^{N_{\max}} \mathrm{ASEP}_{\mathrm{iml}}^{(n)}(\boldsymbol{\mathcal{R}})\right] \gamma^{-(N_{\max}+1)}. \quad (18)$$

In this case, the asymptotic diversity order of the IML detector is equal to $R_{\max}$, i.e., the rank of the signature matrix $\boldsymbol{\mathcal{R}}$, which coincides with the number of potential relays plus one. On the other hand, when $L < N_{\max}+1$, one has $R_{\max} = L$; hence, (16) can be rewritten as

$$\mathrm{ASEP}_{\mathrm{iml}}(\boldsymbol{\mathcal{R}}) \lessapprox \mathrm{ASEP}_{\mathrm{iml}}^{(N_{\max})}(\boldsymbol{\mathcal{R}})\gamma^{-L} + o(\gamma^{-L}). \quad (19)$$

The asymptotic diversity order of the IML detector is now equal to L, i.e., the rank of $\boldsymbol{\mathcal{R}}$, which is equal to the number of virtual antennas in the underlying space–time code. Therefore, we can conclude that the asymptotic diversity order of the system is always given by $R_{\max} = \min(L, N_{\max}+1)$.

Equations (18) and (19) additionally show that randomness in the number of active relays affects the coding gain of the system only when $L \geq N_{\max}+1$. Indeed, in the case of $L < N_{\max}+1$, the coding gain is the same as the case when *all* the potential relays are active in Phase II and depends on the nonzero eigenvalues of $\boldsymbol{\mathcal{R}}^H\boldsymbol{\mathcal{R}}$; in such a case, the coding gain is maximized when the product of the nonzero eigenvalues of $\boldsymbol{\mathcal{R}}^H\boldsymbol{\mathcal{R}}$ is maximized, which is tantamount to solving the constrained optimization problem

$$\boldsymbol{\mathcal{R}}_{\mathrm{opt}} = \arg \max_{\boldsymbol{\mathcal{R}} \in \mathbb{C}^{L\times(N_{\max}+1)}} \prod_{r=1}^{R_{\max}} \mu_r(\boldsymbol{\mathcal{R}}^H\boldsymbol{\mathcal{R}}) \quad (20)$$

subject to $\mathrm{trace}(\boldsymbol{\mathcal{R}}^H\boldsymbol{\mathcal{R}}) = \rho > 0$, where the imposed constraint avoids the trivial solution for which the Frobenius norm of $\boldsymbol{\mathcal{R}}$ is unbounded. Instead, in the case of $L \geq N_{\max}+1$, the coding gain is maximized when the product of the nonzero eigenvalues of $\mathbf{S}\boldsymbol{\mathcal{R}}^H\boldsymbol{\mathcal{R}}\mathbf{S}$ is maximized for all the possible configurations of active relays, which leads to the following constrained optimization problem:

$$\boldsymbol{\mathcal{R}}_{\mathrm{opt}} = \arg \max_{\boldsymbol{\mathcal{R}} \in \mathbb{C}^{L\times(N_{\max}+1)}} \prod_{r=1}^{R(\mathbf{s})} \mu_r(\mathbf{S}\boldsymbol{\mathcal{R}}^H\boldsymbol{\mathcal{R}}\mathbf{S}) \quad (21)$$

subject to $\mathrm{trace}(\mathbf{S}\boldsymbol{\mathcal{R}}^H\boldsymbol{\mathcal{R}}\mathbf{S}) = \rho R(\mathbf{s})/R_{\max}$, for all the $2^{N_{\max}}$ different realizations $\mathbf{s}$ of $\tilde{\mathbf{s}}$. With regard to the solution of (20) and (21), we give the lemma.

Lemma 1: When $L < N_{\max}+1$ and, thus, $R_{\max} = L$, the solution of (20) obeys $\boldsymbol{\mathcal{R}}_{\mathrm{opt}}\boldsymbol{\mathcal{R}}_{\mathrm{opt}}^H = (\rho/L)\mathbf{I}_L$. On the other hand, when $L \geq N_{\max}+1$ and, thus, $R_{\max} = N_{\max}+1$, the solution of (21) is given by $\boldsymbol{\mathcal{R}}_{\mathrm{opt}}^H\boldsymbol{\mathcal{R}}_{\mathrm{opt}} = [\rho/(N_{\max}+1)]\mathbf{I}_{N_{\max}+1}$.

Proof: See Appendix B. ■

It is worth noting that the signatures (20) and (21) cannot be chosen by the relays locally, i.e., in a decentralized manner, but they must be assigned to them by a central unit, i.e., in a centralized fashion. To decentralize the coding method, the nth active relay can choose $\tilde{\mathbf{r}}_n$ at random locally [6], without coordinating with other cooperating relays. The ASEP performance of a randomized scheme can be obtained by evaluating the ensemble average of (18) and (19) with respect to $\tilde{\boldsymbol{\mathcal{R}}}$. We directly defer to [6] for details on how to explicitly calculate such averages in the case of some specific randomization rules, such as real/complex Gaussian, uniform phase, real/complex spherical distribution, and antenna selection.

B. Finite-SNR Analysis of the IML Detector

The numerical results reported in Section V show that the behavior of the finite-SNR diversity order as a function of γ is not significantly affected by the randomness in the number of active relays for moderate-to-high SNR values. Thus, to also simplify the analysis, we refer herein to the case in which all the relays are active in Phase II, i.e., we consider the single realization[10] $\mathbf{s} = \mathbf{1}_{N_{\max}}$ of $\tilde{\mathbf{s}}$. In this case, for a given pair $(\mathbf{a}_k, \mathbf{a}_\ell)$, the finite-SNR diversity order $G_d^{\mathrm{iml}}(\gamma, k, \ell)$ of the IML detector can be obtained from (1), where $\mathrm{APEP}(\gamma)$ is replaced with

$$\mathrm{E}_{\widetilde{\mathbf{m}}, \tilde{\mathbf{s}}=\mathbf{1}_{N_{\max}}, \tilde{\boldsymbol{\mathcal{R}}}=\boldsymbol{\mathcal{R}}} \left\{ \mathrm{E}_{\tilde{\mathbf{g}}|\, \widetilde{\mathbf{m}}, \tilde{\mathbf{s}}=\mathbf{1}_{N_{\max}}, \tilde{\boldsymbol{\mathcal{R}}}=\boldsymbol{\mathcal{R}}} \left[\mathrm{PEP}_{\mathrm{iml}}(\tilde{\mathbf{h}}, \tilde{\mathbf{m}}) \right] \right\}.$$

Accounting for all possible pairwise errors, the finite-SNR diversity order of the IML detector is defined as

$$G_d^{\mathrm{iml}}(\gamma) \triangleq \min_{\substack{k,\ell \in \{1,2,\ldots,|\mathcal{A}|\} \\ \ell \neq k}} G_d^{\mathrm{iml}}(\gamma, k, \ell) \quad (22)$$

whose *exact* expression is given by the following theorem.

Theorem 2 (IML Finite-SNR Diversity Order): Let $\boldsymbol{\Phi}_{k,\ell} \triangleq \boldsymbol{\mathcal{C}}_{k,\ell}\boldsymbol{\mathcal{R}}\boldsymbol{\Sigma}_{\tilde{\mathbf{g}}}\boldsymbol{\mathcal{R}}^H\boldsymbol{\mathcal{C}}_{k,\ell}^H \in \mathbb{C}^{P\times P}$ and $\boldsymbol{\Lambda}_{\mathbf{m}} \triangleq \mathrm{diag}(\lambda^{m_1}/m_1!, \lambda^{m_2}/m_2!, \ldots, \lambda^{m_P}/m_P!) \in \mathbb{R}^{P\times P}$. It results that $G_d^{\mathrm{iml}}(\gamma)$ is given by (23) shown at the bottom of the page, with

$$u_1(\gamma, \theta, \mathbf{m}) \triangleq \det{}^{-1}\left(\mathbf{I}_P + \frac{\gamma}{4\sin^2\theta}\boldsymbol{\Sigma}_{\mathbf{m}}^{-1}\boldsymbol{\Phi}_{k,\ell}\right) \quad (24)$$

$$u_2(\gamma, \theta, \mathbf{m}) \triangleq \mathrm{trace}\left[\left(\frac{4\sin^2\theta}{\gamma}\boldsymbol{\Sigma}_{\mathbf{m}} + \boldsymbol{\Phi}_{k,\ell}\right)^{-1}\boldsymbol{\Phi}_{k,\ell}\right] \quad (25)$$

[10]The generalization of the forthcoming results to an arbitrary realization of the random vector $\tilde{\mathbf{s}}$ is straightforward.

$$G_d^{\mathrm{iml}}(\gamma) = \min_{\substack{k,\ell \in \{1,2,\ldots,|\mathcal{A}|\} \\ \ell \neq k}} \frac{\sum_{m_1=0}^{+\infty}\sum_{m_2=0}^{+\infty}\cdots\sum_{m_P=0}^{+\infty} \det(\boldsymbol{\Lambda}_{\mathbf{m}}) \int_0^{\pi/2} u_1(\gamma,\theta,\mathbf{m}) u_2(\gamma,\theta,\mathbf{m}) d\theta}{\sum_{m_1=0}^{+\infty}\sum_{m_2=0}^{+\infty}\cdots\sum_{m_P=0}^{+\infty} \det(\boldsymbol{\Lambda}_{\mathbf{m}}) \int_0^{\pi/2} u_1(\gamma,\theta,\mathbf{m}) d\theta} \quad (23)$$

where $\text{rank}(\mathbf{\Sigma}_{\mathbf{m}}^{-1}\mathbf{\Phi}_{k,\ell}) = \text{rank}(\mathbf{\Phi}_{k,\ell}) = \text{rank}(\mathcal{C}_{k,\ell}\mathcal{R}) = R_{\max} \leq P$, provided that $P \geq L$.

Proof: See Appendix C. ■

As a first remark regarding Theorem 2, we observe that $\mathbf{\Sigma}_{\mathbf{m}} \succeq [\Gamma/(1+\Gamma)]\mathbf{I}_P$, and thus, one gets

$$\left(\frac{4\Gamma \sin^2\theta}{\gamma(1+\Gamma)}\mathbf{I}_P + \mathbf{\Phi}_{k,\ell}\right)^{-1} \succeq \left(\frac{4\sin^2\theta}{\gamma}\mathbf{\Sigma}_{\mathbf{m}} + \mathbf{\Phi}_{k,\ell}\right)^{-1} \quad (26)$$

which, along with $\sin^2\theta \geq 0$, implies [50] that

$$u_2(\gamma,\theta,\mathbf{m}) \leq \lim_{\theta\to 0} \text{trace}\left\{\left[\frac{4\Gamma\sin^2\theta}{\gamma(1+\Gamma)}\mathbf{I}_P + \mathbf{\Phi}_{k,\ell}\right]^{-1}\mathbf{\Phi}_{k,\ell}\right\}. \quad (27)$$

By invoking the limit formula and the properties of the Moore–Penrose inverse [51], one has

$$\begin{aligned} u_2(\gamma,\theta,\mathbf{m}) &\leq \text{trace}\left[\left(\mathbf{\Sigma}_{\tilde{\mathbf{g}}}^{1/2}\mathcal{R}^H\mathcal{C}_{k,\ell}^H\right)^{\dagger}\left(\mathbf{\Sigma}_{\tilde{\mathbf{g}}}^{1/2}\mathcal{R}^H\mathcal{C}_{k,\ell}^H\right)\right] \\ &= \text{trace}\left[\left(\mathcal{R}^H\mathcal{C}_{k,\ell}^H\right)^{\dagger}\left(\mathcal{R}^H\mathcal{C}_{k,\ell}^H\right)\right] \\ &= \text{rank}\left[\left(\mathcal{R}^H\mathcal{C}_{k,\ell}^H\right)^{\dagger}\left(\mathcal{R}^H\mathcal{C}_{k,\ell}^H\right)\right] \\ &= \text{rank}(\mathcal{C}_{k,\ell}\mathcal{R}) = R_{\max}. \end{aligned} \quad (28)$$

The first consequence of (28) is that $G_d^{\text{iml}}(\gamma) \leq R_{\max}$, where we recall that $R_{\max}$ is the asymptotic diversity order (see Section III-A). Moreover, the functions $u_1(\gamma,\theta,\mathbf{m})$ and $u_2(\gamma,\theta,\mathbf{m})$ are nondecreasing and nonincreasing, respectively, with respect to $\mathbf{m} = [m_1, m_2, \ldots, m_P] \in \mathbb{N}^P$, i.e., let $\overline{\mathbf{m}} \triangleq [\overline{m}_1, \overline{m}_2, \ldots, \overline{m}_P] \in \mathbb{N}^P$, if $m_p \leq \overline{m}_p$ for $p \in \{1,2,\ldots,P\}$, then $\mathbf{\Sigma}_{\overline{\mathbf{m}}} \succeq \mathbf{\Sigma}_{\mathbf{m}}$, implying [50] that $u_1(\gamma,\theta,\mathbf{m}) \leq u_1(\gamma,\theta,\overline{\mathbf{m}})$ and $u_2(\gamma,\theta,\mathbf{m}) \geq u_2(\gamma,\theta,\overline{\mathbf{m}})$. With regard to the behavior of $G_d^{\text{iml}}(\gamma)$ for finite values of the SNR, it is seen that $u_1(\gamma,\theta,\mathbf{m})$ is a nonincreasing function with respect to γ, i.e., if $\gamma_1 < \gamma_2$, then $u_1(\gamma_1,\theta,\mathbf{m}) \geq u_1(\gamma_2,\theta,\mathbf{m})$, whereas the function $u_2(\gamma,\theta,\mathbf{m})$ is nondecreasing with respect to γ, i.e., $u_2(\gamma_1,\theta,\mathbf{m}) \leq u_2(\gamma_2,\theta,\mathbf{m})$ if $\gamma_1 < \gamma_2$. In highly impulsive noise cases, this fact does not allow $G_d^{\text{iml}}(\gamma)$ to monotonously increase for raising values of γ, by leading to a fluctuating trend.

To gain more insight into this behavior, let us consider an M-term truncated version of the MCA noise model, with $M \geq 2$, which has been shown to be a good approximation for several scenarios of interest [45]. In this case, diversity order (23) can be approximated as (29) shown at the bottom of the page, where we have additionally used the trapezoid rule[11] to approximate the integrals in (23). Let us consider the cases of near-Gaussian and highly impulsive noise separately.

[11]Let $b > a$ and $f(x) \geq 0$, the following approximation $\int_a^b f(x)dx \approx (1/2)(b-a)[f(a)+f(b)]$ is called the trapezoid rule.

1) Near-Gaussian Noise Case: Under the assumption that $(M-1)/\lambda \ll \Gamma$, i.e., the noise is near Gaussian, it results from (4) that

$$\sigma_{m_p}^2 \approx \sigma_0^2 = \frac{\Gamma}{1+\Gamma} \quad (30)$$

for each $m_p \in \{0,1,\ldots,M-1\}$ and $p \in \{1,2,\ldots,P\}$. Thus, it follows from (24), (25), and (29) that

$$G_d^{\text{iml}}(\gamma) \approx \min_{\substack{k,\ell\in\{1,2,\ldots,|\mathcal{A}|\}\\ \ell\neq k}} \text{trace}\left[\left(\frac{4\sigma_0^2}{\gamma}\mathbf{I}_P + \mathbf{\Phi}_{k,\ell}\right)^{-1}\cdot\mathbf{\Phi}_{k,\ell}\right] \quad (31)$$

which is a nondecreasing function of the SNR approaching its asymptotic value $R_{\max}$ as $\gamma \to +\infty$.

As a case study, let us assume that: 1) the source and all the relays are (approximatively) at the same location, i.e., $\mathbf{\Sigma}_{\tilde{\mathbf{g}}} = \sigma_{\tilde{g}_0}^2\mathbf{I}_{N_{\max}+1}$; 2) $L \leq N_{\max}+1$ and $\mathcal{R}_{\text{opt}}\mathcal{R}_{\text{opt}}^H = (\rho/L)\mathbf{I}_L$ (see Lemma 1)[12]; and 3) the space–time code is complex orthogonal [16], i.e., $\mathcal{C}^H(\mathbf{a})\mathcal{C}(\mathbf{a}) = \|\mathbf{a}\|^2\mathbf{I}_L, \forall\,\mathbf{a} \in \mathbb{C}^K - \{\mathbf{0}_K\}$. Under these assumptions, it results that $\mathbf{\Phi}_{k,\ell} = [(\sigma_{\tilde{g}_0}^2\rho)/L]\mathcal{C}_{k,\ell}\mathcal{C}_{k,\ell}^H$, with $L \leq P$, and hence, it follows from (13) that[13]

$$G_d^{\text{iml}}(\gamma) \approx \frac{L\tau\gamma}{L+\tau\gamma}, \quad \text{with } \tau \triangleq \frac{\rho(1+\Gamma)\Delta_{\min}^2\sigma_{\tilde{g}_0}^2}{4\Gamma} \quad (32)$$

where $\Delta_{\min}$ denotes the minimum distance between the blocks of symbols in $\mathcal{A}$. Equation (32) clearly shows that $G_d^{\text{iml}}(\gamma)$ monotonously increases as a function of γ for reaching the asymptotic value $R_{\max} = L$.

2) Highly Impulsive Noise Case: Under the assumption that $\lambda\Gamma \ll 1$ with $\Gamma < 1$, i.e., the noise is highly impulsive, it results from (4) that

$$\sigma_{m_p}^2 \approx \frac{m_p}{\lambda(1+\Gamma)} \quad (33)$$

for each $m_p \in \{1,2,\ldots,M-1\}$ and $p \in \{1,2,\ldots,P\}$. In this case, using (33) and neglecting all the summands that tend to zero faster than λ, the diversity order given by (29) can be further approximated as in (34) shown at the bottom of the next page, where $\mathbf{e}_p \in \mathbb{C}^P$ has the only nonzero entry $\{\mathbf{e}_p\}_p = 1$, for each $p \in \{1,2,\ldots,P\}$. To streamline our analysis, let us focus on the case study considered in Section III-B1, with

[12]The case of $L > N_{\max}+1$ and $\mathcal{R}_{\text{opt}}^H\mathcal{R}_{\text{opt}} = [\rho/(N_{\max}+1)]\mathbf{I}_{N_{\max}+1}$ can be treated in a similar way.

[13]We have used the three facts that 1) $(a\mathbf{I}_P + \mathcal{C}_{k,\ell}\mathcal{C}_{k,\ell}^H)^{-1} = a^{-1}[\mathbf{I}_P - \mathcal{C}_{k,\ell}(\mathcal{C}_{k,\ell}^H\mathcal{C}_{k,\ell} + a\mathbf{I}_L)^{-1}\mathcal{C}_{k,\ell}^H]$, where a is an arbitrary constant; 2) $\text{trace}(\mathcal{C}_{k,\ell}\mathcal{C}_{k,\ell}^H) = \text{trace}(\mathcal{C}_{k,\ell}^H\mathcal{C}_{k,\ell})$; and 3) $\mathcal{C}_{k,\ell}^H\mathcal{C}_{k,\ell} = \|\mathbf{a}_k - \mathbf{a}_\ell\|^2\mathbf{I}_L$.

$$G_d^{\text{iml}}(\gamma) \approx \min_{\substack{k,\ell\in\{1,2,\ldots,|\mathcal{A}|\}\\ \ell\neq k}} \frac{\sum_{m_1=0}^{M-1}\sum_{m_2=0}^{M-1}\cdots\sum_{m_P=0}^{M-1}\det(\mathbf{\Lambda}_{\mathbf{m}})u_1(\gamma,\pi/2,\mathbf{m})u_2(\gamma,\pi/2,\mathbf{m})}{\sum_{m_1=0}^{M-1}\sum_{m_2=0}^{M-1}\cdots\sum_{m_P=0}^{M-1}\det(\mathbf{\Lambda}_{\mathbf{m}})u_1(\gamma,\pi/2,\mathbf{m})} \quad (29)$$

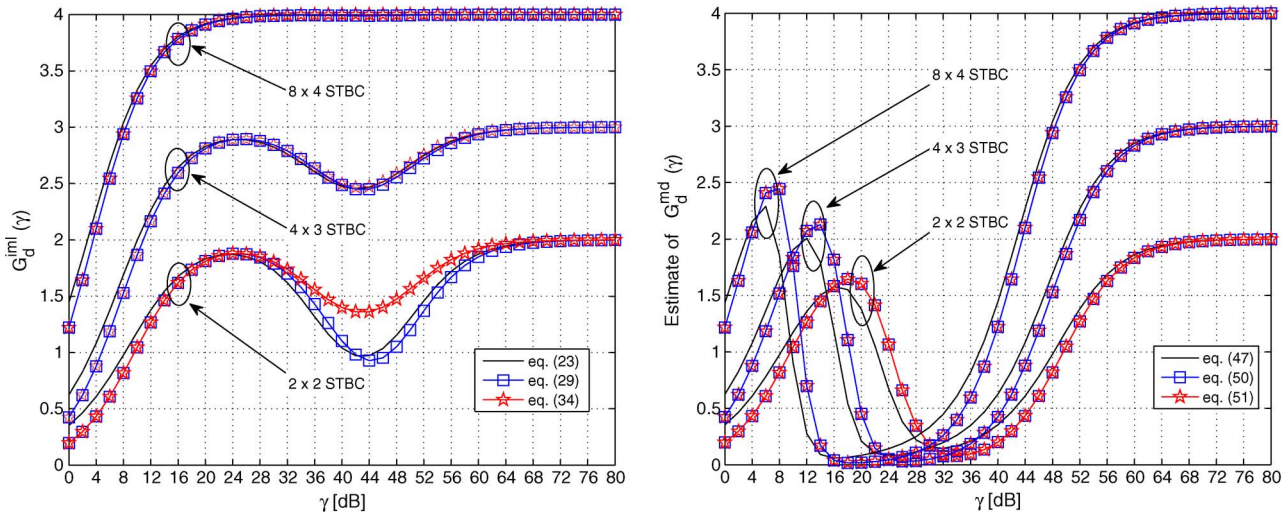

Fig. 1. Very highly impulsive noise. Diversity orders (left-side plot) $G_d^{\mathrm{iml}}(\gamma)$ and (right-side plot) $\widehat{G}_d^{\mathrm{md}}(\gamma)$ versus γ for different STBC rules (Examples 1 and 2: QPSK signaling, $N_{\max} = L-1$, $M=2$, $\lambda = 10^{-3}$, $\Gamma = 0.1$, and $\sigma_{\tilde{g}_0}^2 \triangleq 10^{-2}$).

the additional assumption that the space–time code is square $(L=P)$,[14] i.e., when $\mathbf{\Phi}_{k,\ell} = [(\sigma_{\tilde{g}_0}^2\rho)/L]\|\mathbf{a}_k - \mathbf{a}_\ell\|^2\mathbf{I}_L$. In this case, it can be seen that (24) and (25) simplify to

$$u_1(\gamma, \pi/2, \mathbf{e}_p) = \prod_{p=1}^{L}\left(1 + \frac{\rho\|\mathbf{a}_k - \mathbf{a}_\ell\|^2\sigma_{\tilde{g}_0}^2}{4L}\frac{\gamma}{\sigma_{m_p}^2}\right)^{-1} \quad (35)$$

$$u_2(\gamma, \pi/2, \mathbf{e}_p) = \sum_{p=1}^{L}\left(1 + \frac{4L}{\rho\|\mathbf{a}_k - \mathbf{a}_\ell\|^2\sigma_{\tilde{g}_0}^2}\frac{\sigma_{m_p}^2}{\gamma}\right)^{-1} \quad (36)$$

for each $p \in \{1, 2, \ldots, P\}$. By substituting (35) and (36) in (34) and using (33), after some algebraic rearrangements, one has the expression

$$G_d^{\mathrm{iml}}(\gamma) \approx \frac{\frac{\tau\gamma}{\left(1+\frac{\tau}{L}\gamma\right)^2} + \frac{L\lambda}{1+\frac{\tau}{L}\lambda\Gamma\gamma}\left[\frac{(L-1)\frac{\tau}{L}\gamma}{1+\frac{\tau}{L}\gamma} + \frac{\frac{\tau}{L}\lambda\Gamma\gamma}{1+\frac{\tau}{L}\lambda\Gamma\gamma}\right]}{\frac{1}{1+\frac{\tau}{L}\gamma} + \frac{L\lambda}{1+\frac{\tau}{L}\lambda\Gamma\gamma}}. \quad (37)$$

Example 1: The exact value of $G_d^{\mathrm{iml}}(\gamma)$ in (23) and its approximations (29) and (34) are shown in Fig. 1 (left-side plot) as a function of γ for different STBC rules, with QPSK signaling, i.e., $\tilde{a}_k = \{\pm 1/\sqrt{2} \pm j/\sqrt{2}\}$, for $k \in \{1, 2, \ldots, K\}$, $N_{\max} = L-1$, $M=2$, $\lambda = 10^{-3}$, $\Gamma = 0.1$, and $\sigma_{\tilde{g}_0}^2 \triangleq d_{\mathrm{SD}}^{-2}$, where $d_{\mathrm{SD}} = 10$ m is the distance between the source and the destination. Specifically, we considered as STBC rules the full-rate Alamouti complex code [47] of order $L = K = P = 2$, the complex orthogonal code of order $L = K = 3$ with code rate $K/P = 3/4$ [48], and, finally, the complex orthogonal code of order $L = K = 4$ with code rate $K/P = 4/8 = 1/2$ [49, Example 4.7.1]. In all these cases, the asymptotic diversity order is $R_{\max} = L$. It is seen that, for the 2×2 and 4×3 STBC matrices, the diversity order rises and falls between a maximum and a minimum before starting to monotonically increase for reaching the asymptotic values 2 and 3, respectively; such fluctuating behavior completely disappears in the case of the 8×4 STBC matrix, where $G_d^{\mathrm{iml}}(\gamma)$ monotonously reaches its asymptotic value 4. A satisfactory agreement among (23), (29), and (34) can be observed. With reference to the Alamouti code, the simple formula (37), which exactly coincides with (34) for $L = P$, accurately captures the behavior of $G_d^{\mathrm{iml}}(\gamma)$, by showing only a slight discrepancy in the neighborhood of the local minimum.

After some straightforward but tedious calculations, it is shown that $G_d^{\mathrm{iml}}(\gamma)$ given by (37) has local maximum and minimum points at

$$\gamma_{\max}^{\mathrm{iml}} \approx \frac{L}{\tau\sqrt{\lambda}}$$
$$\gamma_{\min}^{\mathrm{iml}} \approx \frac{\sqrt{L}}{\lambda\tau\sqrt{\Gamma}} \quad (38)$$

respectively, which allow directly linking the extrema of $G_d^{\mathrm{iml}}(\gamma)$ to the parameters of noise and STBC. In the case of the Alamouti code (see Example 1), (38) gives $\gamma_{\max}^{\mathrm{iml}} = 24.56$ dB and $\gamma_{\min}^{\mathrm{iml}} = 43$ dB, whereas their corresponding exact values numerically obtained from (23) are 24 and 42 dB, respectively.

[14] With respect to their nonsquare counterparts, square complex orthogonal code matrices require a much smaller processing delay, with the consequence of a slightly smaller maximum code rate [46].

$$G_d^{\mathrm{iml}}(\gamma) \approx \min_{\substack{k,\ell\in\{1,2,\ldots,|\mathcal{A}|\}\\ \ell\neq k}} \frac{u_1(\gamma,\pi/2,\mathbf{0}_P)u_2(\gamma,\pi/2,\mathbf{0}_P) + \lambda\sum_{p=1}^{P} u_1(\gamma,\pi/2,\mathbf{e}_p)u_2(\gamma,\pi/2,\mathbf{e}_p)}{u_1(\gamma,\pi/2,\mathbf{0}_P) + \lambda\sum_{p=1}^{P} u_1(\gamma,\pi/2,\mathbf{e}_p)} \quad (34)$$

IV. Performance Analysis of the Minimum-Distance Detector

The diversity scheme considered in Section III requires that the destination node implements decision rule (8) for ML detection of $\tilde{\mathbf{a}}$, by resorting to the M-term truncation of the noise pdf. For those systems with simple terminal units such as wireless sensor networks and practical ad hoc or multihop wireless networks, this processing may be too computationally expensive for large values of K, M, P, and/or $|\mathcal{A}|$. Herein, we investigate the performance of a suboptimal scheme, which is based on the MD decision rule and, thus, involves a less processing burden at the destination.

Given $\tilde{\mathbf{h}} = \mathbf{h}$, the MD decision rule is defined as follows:

$$\widehat{\mathbf{a}}_{\mathrm{md}} = \arg \min_{k \in \{1,2,\ldots,|\mathcal{A}|\}} \|\mathbf{y} - \boldsymbol{\mathcal{C}}_k \mathbf{h}\|^2 \tag{39}$$

which turns out to be optimal (in the minimum-error-probability sense) when the noise $\tilde{d}_p$ boils down to a circular symmetric complex Gaussian RV, for each $p \in \{1, 2, \ldots, P\}$. For the noise model at hand, this happens for asymptotically large values of λ and/or Γ.

In what follows, we study the cases of the high- and finite-SNR regimes separately, by again keeping the signature matrix $\tilde{\boldsymbol{\mathcal{R}}}$ fixed to $\boldsymbol{\mathcal{R}}$, with rank $R_{\max} = \min(L, N_{\max} + 1)$.

A. Analysis of the MD Detector in the High-SNR Region

As previously done in the IML case, for sufficiently high SNR values, the ASEP at the output of the MD decoder, given $\tilde{\mathbf{s}} = \mathbf{s}$, can be approximatively expressed as (40) shown at the bottom of the page, where, from (39), the PEP of the MD detector $\mathrm{PEP}_{\mathrm{md}}(\tilde{\mathbf{h}}, \tilde{\mathbf{m}}) \triangleq P(\{\mathbf{a}_k \to \mathbf{a}_\ell\}_{\mathrm{md}} | \tilde{\mathbf{h}}, \tilde{\mathbf{m}})$, conditioned on $\tilde{\mathbf{h}} = \mathbf{h}$ and $\tilde{\mathbf{m}} = \mathbf{m}$, is given by

$$\begin{aligned}
\mathrm{PEP}_{\mathrm{md}}(\mathbf{h}, \mathbf{m}) &= \mathrm{Q}\left(\frac{\|\boldsymbol{\mathcal{C}}_{k,\ell}\mathbf{h}\|^2}{\sqrt{2\sigma^2} \left\| \boldsymbol{\Sigma}_{\mathbf{m}}^{1/2} \boldsymbol{\mathcal{C}}_{k,\ell}\mathbf{h} \right\|} \right) \\
&\leq \mathrm{Q}\left(\frac{\|\boldsymbol{\mathcal{C}}_{k,\ell}\mathbf{h}\|}{\sqrt{2\sigma^2 \mu_1(\boldsymbol{\Sigma}_{\mathbf{m}})}} \right) \\
&= \frac{1}{\pi} \int_0^{\pi/2} \exp\left(-\frac{\mathbf{h}^H \boldsymbol{\mathcal{C}}_{k,\ell}^H \boldsymbol{\mathcal{C}}_{k,\ell}\mathbf{h}}{4\sigma^2 \mu_1(\boldsymbol{\Sigma}_{\mathbf{m}}) \sin^2\theta} \right) d\theta
\end{aligned} \tag{41}$$

where the Rayleigh–Ritz inequality $\|\boldsymbol{\Sigma}_{\mathbf{m}}^{1/2} \boldsymbol{\mathcal{C}}_{k,\ell}\mathbf{h}\|^2 \leq \mu_1(\boldsymbol{\Sigma}_{\mathbf{m}}) \|\boldsymbol{\mathcal{C}}_{k,\ell}\mathbf{h}\|^2$ has been invoked [50]. It is worth noting that by directly comparing (10) and (41), it results to the fact that if the number of impulses affecting the destination is identical in each symbol period, i.e., $\boldsymbol{\Sigma}_{\mathbf{m}} = \sigma_{m_1}^2 \mathbf{I}_P$, the MD detector has the same PEP performance as the IML detector. More generally, it results that $\mathrm{PEP}_{\mathrm{ml}}(\mathbf{h}) \leq \mathrm{PEP}_{\mathrm{md}}(\mathbf{h}, \mathbf{m})$, which is a consequence of the fact that the ML detector minimizes the probability of error when the specific realization of $\widetilde{\mathbf{m}}$ is unknown. Given $\tilde{\boldsymbol{\mathcal{R}}} = \boldsymbol{\mathcal{R}}$ and $\tilde{\mathbf{s}} = \mathbf{s}$, the ASEP performance of the MD detector in the high-SNR region is given by the following theorem.

Theorem 3 (MD ASEP for a Fixed Number of Active Relays): Under the same assumptions of Theorem 1, it results that

$$\begin{aligned}
\mathrm{ASEP}_{\mathrm{md}}(\boldsymbol{\mathcal{R}}, \mathbf{s}) \lessapprox\ & \Psi\left(\lambda, R(\mathbf{s})\right) \Upsilon\left(N(\mathbf{s})\right) \\
& \cdot \left[\prod_{r=1}^{R(\mathbf{s})} \frac{1}{\mu_r(\mathbf{S}\boldsymbol{\mathcal{R}}^H \boldsymbol{\mathcal{R}}\mathbf{S})} \right] \gamma^{-R(\mathbf{s})}
\end{aligned} \tag{42}$$

where

$$\Psi\left(\lambda, R(\mathbf{s})\right) \triangleq P\mathrm{E}\left[\left(\frac{\widetilde{m}_p \lambda^{-1} + \Gamma}{1 + \Gamma} \right)^{R(\mathbf{s})} \right] \tag{43}$$

whereas $\Upsilon(N(\mathbf{s}))$ and γ have been defined in Theorem 1.

Proof: See Appendix D. ■

It is apparent from Theorem 1 and Theorem 3 that the upper bounds (12) and (42) on the ASEP performance of the IML and MD detectors, respectively, differ only in the presence of the function $\Psi(\lambda, R(\mathbf{s}))$. Therefore, following the same steps done in Section III-A, one obtains

$$\begin{aligned}
\mathrm{ASEP}_{\mathrm{md}}(\boldsymbol{\mathcal{R}}) &\triangleq \mathrm{E}_{\tilde{\mathbf{s}}|\tilde{\boldsymbol{\mathcal{R}}}=\boldsymbol{\mathcal{R}}} \left[\mathrm{ASEP}_{\mathrm{md}}(\tilde{\boldsymbol{\mathcal{R}}}, \tilde{\mathbf{s}}) \right] \\
&\lessapprox \sum_{n=0}^{N_{\max}} \mathrm{ASEP}_{\mathrm{md}}^{(n)}(\boldsymbol{\mathcal{R}}) \gamma^{-[\min(L, n+1) + N_{\max} - n]}
\end{aligned} \tag{44}$$

where $\mathrm{ASEP}_{\mathrm{md}}^{(n)}(\boldsymbol{\mathcal{R}}) \triangleq \Psi(\lambda, R(\mathbf{s})) \mathrm{ASEP}_{\mathrm{iml}}^{(n)}(\boldsymbol{\mathcal{R}})$, which, compared with (16), shows that the IML and MD detectors have the same asymptotic diversity order $R_{\max}$ but different coding gains. In particular, it is shown in [29, Appendix I] that $\Psi(\lambda, R(\mathbf{s})) \geq 1$ and, additionally, that the function $\Psi(\lambda, R(\mathbf{s}))$ is monotonically decreasing in λ and monotonically increasing in $R(\mathbf{s})$. In other words, the coding gain of the MD detector is smaller than or equal to that of the IML detector, and the performance penalty enlarges for increasing values of $R(\mathbf{s})$; on the other hand, for a fixed value of $R(\mathbf{s})$, such a penalty is negligible in the case of near-Gaussian noise, i.e., for high values of λ, whereas it becomes significant if the noise is highly impulsive, i.e., for small values of λ. However, the signature matrix $\boldsymbol{\mathcal{R}}_{\mathrm{opt}}$ given by (20) and (21) also maximizes the coding gain of the system with MD detection at the destination when $L < N_{\max} + 1$ and $L \geq N_{\max} + 1$, respectively. The ASEP performance of a randomized scheme with a specific probability distribution directly follows from (44) by using the results in [6].

$$\mathrm{ASEP}_{\mathrm{md}}(\boldsymbol{\mathcal{R}}, \mathbf{s}) \approx N_e \cdot \max_{\substack{k, \ell \in \{1,2,\ldots,|\mathcal{A}|\} \\ \ell \neq k}} \mathrm{E}_{\widetilde{\mathbf{m}}|\tilde{\mathbf{s}}=\mathbf{s}, \tilde{\boldsymbol{\mathcal{R}}}=\boldsymbol{\mathcal{R}}} \left\{ \mathrm{E}_{\tilde{\mathbf{g}}|\widetilde{\mathbf{m}}, \tilde{\mathbf{s}}=\mathbf{s}, \tilde{\boldsymbol{\mathcal{R}}}=\boldsymbol{\mathcal{R}}} \left[\mathrm{PEP}_{\mathrm{md}}(\tilde{\mathbf{h}}, \tilde{\mathbf{m}}) \right] \right\} \tag{40}$$

B. Finite-SNR Analysis of the MD Detector

As done for the IML detector in Section III-B, the finite-SNR performance of the MD detector is evaluated by considering the single realization $\mathbf{s}=\mathbf{1}_{N_{\max}}$ of the vector $\tilde{\mathbf{s}}$. In this case, for a given pair $(\mathbf{a}_k,\mathbf{a}_\ell)$, the exact expression of the finite-SNR diversity order $G_d^{\mathrm{md}}(\gamma,k,\ell)$ can be obtained from (1), where APEP(γ) is replaced with

$$\mathrm{E}_{\widetilde{\mathbf{m}}\,|\mathbf{s}=\mathbf{1}_{N_{\max}},\tilde{\boldsymbol{\mathcal{R}}}=\boldsymbol{\mathcal{R}}}\left\{\mathrm{E}_{\tilde{\mathbf{g}}|\,\widetilde{\mathbf{m}},\mathbf{s}=\mathbf{1}_{N_{\max}},\tilde{\boldsymbol{\mathcal{R}}}=\boldsymbol{\mathcal{R}}}\left[\mathrm{PEP}_{\mathrm{md}}(\tilde{\mathbf{h}},\tilde{\mathbf{m}})\right]\right\}.$$

In this respect, by resorting to the upper bound in (41), we observe that

$$\mathrm{E}_{\widetilde{\mathbf{m}}\,|\mathbf{s}=\mathbf{1}_{N_{\max}},\tilde{\boldsymbol{\mathcal{R}}}=\boldsymbol{\mathcal{R}}}\left\{\mathrm{E}_{\tilde{\mathbf{g}}|\,\widetilde{\mathbf{m}},\mathbf{s}=\mathbf{1}_{N_{\max}},\tilde{\boldsymbol{\mathcal{R}}}=\boldsymbol{\mathcal{R}}}\left[\mathrm{PEP}_{\mathrm{md}}(\tilde{\mathbf{h}},\tilde{\mathbf{m}})\right]\right\}$$

$$\leq\frac{P}{\pi}\sum_{m_p=0}^{+\infty}p_{\widetilde{m}_p}(m_p)\int_0^{\pi/2}\det{}^{-1}\left(\mathbf{I}_P+\gamma\frac{\boldsymbol{\Phi}_{k,\ell}}{4\sigma_{m_p}^2\sin^2\theta}\right)d\theta \quad (45)$$

where we have used (69) in Appendix D, with $\boldsymbol{\Phi}_{k,\ell}$ defined in Theorem 2, and the facts that $\mu_1(\boldsymbol{\Sigma}_{\tilde{\mathbf{m}}})=\max(\sigma_{\tilde{m}_1}^2,\sigma_{\tilde{m}_2}^2,\ldots,\sigma_{\tilde{m}_P}^2)$ and the pmf of $\tilde{m}\triangleq\max(\tilde{m}_1,\tilde{m}_2,\ldots,\tilde{m}_P)$ can be upper bounded as in (72) in Appendix D. Similarly to (22), the finite-SNR diversity order of the MD detector is defined as

$$G_d^{\mathrm{md}}(\gamma)\triangleq\min_{\substack{k,\ell\in\{1,2,\ldots,|\mathcal{A}|\}\\ \ell\neq k}}G_d^{\mathrm{md}}(\gamma,k,\ell). \quad (46)$$

To simplify the mathematical derivations, an estimate $\widehat{G}_d^{\mathrm{md}}(\gamma)$ of $G_d^{\mathrm{md}}(\gamma)$ is evaluated in the following theorem by using (1) and replacing APEP(γ) with the upper bound in (45). The good agreement between $\widehat{G}_d^{\mathrm{md}}(\gamma)$ and $G_d^{\mathrm{md}}(\gamma)$ is demonstrated in Section V through Monte Carlo simulations.

Theorem 4 (Estimate of the MD Finite-SNR Diversity Order): It results that $\widehat{G}_d^{\mathrm{md}}(\gamma)$ is given by (47) shown at the bottom of the page, with

$$v_1(\gamma,\theta,m_p)\triangleq\det{}^{-1}\left(\mathbf{I}_P+\frac{\gamma}{4\sigma_{m_p}^2\sin^2\theta}\boldsymbol{\Phi}_{k,\ell}\right) \quad (48)$$

$$v_2(\gamma,\theta,m_p)\triangleq\mathrm{trace}\left[\left(\frac{4\sigma_{m_p}^2\sin^2\theta}{\gamma}\mathbf{I}_P+\boldsymbol{\Phi}_{k,\ell}\right)^{-1}\boldsymbol{\Phi}_{k,\ell}\right] \quad (49)$$

where $\boldsymbol{\Phi}_{k,\ell}$ has been defined in Theorem 2.

Proof: The proof is omitted since it can be carried out by proceeding as in Appendix C. ■

Similarly to (27) and (28), it can be shown that $v_2(\gamma,\theta,m_p)\leq R_{\max}$, which implies that $\widehat{G}_d^{\mathrm{md}}(\gamma)\leq R_{\max}$, where $R_{\max}$ is the asymptotic diversity order. Moreover, functions $v_1(\gamma,\theta,m_p)$ and $v_2(\gamma,\theta,m_p)$ are nondecreasing and nonincreasing, respectively, with respect to $m_p\in\mathbb{N}$.

As previously done for the IML detector, we approximate diversity order (47) by considering an M-term truncated version of the MCA noise model, with $M\geq 2$, thus obtaining (50) shown at the bottom of the page, where we have again used the trapezoid rule to approximate the integrals in (47). In the sequel, the cases of near-Gaussian and highly impulsive noise are separately studied.

1) Near-Gaussian Noise Case: If $(M-1)/\lambda\ll\Gamma$, approximation (30) holds, and then, it follows from (48)–(50) that $\widehat{G}_d^{\mathrm{md}}(\gamma)\approx G_d^{\mathrm{iml}}(\gamma)$, where $G_d^{\mathrm{iml}}(\gamma)$ is given by (13). In other words, when the noise is near Gaussian, the MD and IML detectors achieve the same finite-SNR diversity order, which is a monotonous increasing function of the SNR [see also the particular case (32)].

2) Highly Impulsive Noise Case: If $\lambda\Gamma\ll 1$ with $\Gamma<1$, approximation (33) holds, and hence, neglecting all the summands in (50) that tend to zero faster than λ, one obtains (51) shown at the bottom of the next page. Under the same assumptions for which (35) and (36) hold, (48) and (49) boil down to[15]

$$v_1(\gamma,\pi/2,m_p)=\left(1+\frac{\rho\|\mathbf{a}_k-\mathbf{a}_\ell\|^2\sigma_{\tilde{g}_0}^2}{4L}\frac{\gamma}{\sigma_{m_p}^2}\right)^{-L} \quad (52)$$

$$v_2(\gamma,\pi/2,m_p)=L\left(1+\frac{4L}{\rho\|\mathbf{a}_k-\mathbf{a}_\ell\|^2\sigma_{\tilde{g}_0}^2}\frac{\sigma_{m_p}^2}{\gamma}\right)^{-1}. \quad (53)$$

[15]Additionally, such expressions also hold if the complex orthogonal code matrix is nonsquare, i.e., $L<P$.

$$\widehat{G}_d^{\mathrm{md}}(\gamma)=\min_{\substack{k,\ell\in\{1,2,\ldots,|\mathcal{A}|\}\\ \ell\neq k}}\frac{\sum_{m_p=0}^{+\infty}\frac{\lambda^{m_p}}{m_p!}\int_0^{\pi/2}v_1(\gamma,\theta,m_p)v_2(\gamma,\theta,m_p)d\theta}{\sum_{m_p=0}^{+\infty}\frac{\lambda^{m_p}}{m_p!}\int_0^{\pi/2}v_1(\gamma,\theta,m_p)d\theta} \quad (47)$$

$$\widehat{G}_d^{\mathrm{md}}(\gamma)\approx\min_{\substack{k,\ell\in\{1,2,\ldots,|\mathcal{A}|\}\\ \ell\neq k}}\frac{\sum_{m_p=0}^{M-1}\frac{\lambda^{m_p}}{m_p!}v_1(\gamma,\pi/2,m_p)v_2(\gamma,\pi/2,m_p)}{\sum_{m_p=0}^{M-1}\frac{\lambda^{m_p}}{m_p!}v_1(\gamma,\pi/2,m_p)} \quad (50)$$

By substituting (52) and (53) in (51), one obtains

$$\widehat{G}_d^{\mathrm{md}}(\gamma) \approx \frac{\frac{\tau\gamma}{\left(1+\frac{\tau}{L}\gamma\right)^{L+1}} + \frac{\tau\lambda^2\Gamma\gamma}{\left(1+\frac{\tau}{L}\lambda\Gamma\gamma\right)^{L+1}}}{\frac{1}{\left(1+\frac{\tau}{L}\gamma\right)^{L}} + \frac{\lambda}{\left(1+\frac{\tau}{L}\lambda\Gamma\gamma\right)^{L}}}. \tag{54}$$

Example 2: The diversity order $\widehat{G}_d^{\mathrm{md}}(\gamma)$ given by (47) and its approximations (50) and (51) are shown in Fig. 1 (right-side plot) as a function of γ, by using the same setting of Example 1. All the curves show a very good agreement between estimated and approximate results. We recall that the simple formula (54) exactly coincides with (51) for $L = P$. It is apparent that, as in the IML case (see left-side plot in Fig. 1), function $\widehat{G}_d^{\mathrm{md}}(\gamma)$ is characterized by a fluctuating trend. However, $\widehat{G}_d^{\mathrm{md}}(\gamma)$ exhibits wider fluctuations than that of the IML detector, which do not smooth as $R_{\max}$ increases, thus deteriorating the system performance; differently from the IML case, it is worth noting that the diversity order of the MD detector can be smaller than 1 over a wide region of SNR values, i.e., $\widehat{G}_d^{\mathrm{md}}(\gamma) < 1$ for $\gamma_{\mathrm{lower}}^{\mathrm{md}} < \gamma < \gamma_{\mathrm{upper}}^{\mathrm{md}}$.

Starting from (54) and putting aside the threshold $\gamma_{\mathrm{lower}}^{\mathrm{md}}$ that falls into an SNR regime of no practical interest in many communication scenarios, it can be verified that

$$\gamma_{\mathrm{upper}}^{\mathrm{md}} = \frac{L}{\tau\lambda\Gamma(L-1)} \tag{55}$$

which diminishes for increasing values of L. In the case of the Alamouti code (Example 1), (55) gives $\gamma_{\mathrm{upper}}^{\mathrm{md}} = 49.58$ dB, whereas its corresponding exact value numerically obtained from (47) is 50 dB.

V. Monte Carlo Performance Analysis

We present a Monte Carlo numerical analysis of the cooperative schemes considered in Sections III and IV to validate and complete our theoretical performance analyses, with reference to both centralized and decentralized relaying, denoted by subscripts "C" and "D" in the plots, respectively. In the former case, the signature matrix $\boldsymbol{\mathcal{R}}$ is chosen according to Lemma 1, i.e., the source and each active relay transmit a preassigned column of the STBC matrix $\boldsymbol{\mathcal{C}}(\tilde{\mathbf{a}})$; in the latter case, $\boldsymbol{\mathcal{R}} = [\rho/(LN)]^{1/2}\tilde{\boldsymbol{\mathcal{N}}}$, where the entries of $\tilde{\boldsymbol{\mathcal{N}}} \in \mathbb{C}^{L\times N}$ are i.i.d. $\mathcal{CN}(0,1)$, i.e., the source and each active relay transmit a linear combination of the columns of $\boldsymbol{\mathcal{C}}(\tilde{\mathbf{a}})$ with complex Gaussian coefficients.

In all the experiments, we adopted the following simulation setting. All the relay nodes are uniformly and independently distributed in a circle of 10-m radius centered around the destination node. The distance d_{SD} between the source and the destination is 10 m, and $\sigma_{\tilde{g}_0}^2 \triangleq d_{\mathrm{SD}}^{-2}$. For $n \in \{1, 2, \ldots, N_{\max}\}$, we assumed that $\sigma_{\tilde{f}_n}^2 \triangleq d_{\mathrm{SR},n}^{-2}$ and $\sigma_{\tilde{g}_n}^2 \triangleq d_{\mathrm{RD},n}^{-2}$, where $d_{\mathrm{SR},n}$ is the distance between the source and the nth relay, whereas $d_{\mathrm{RD},n}$ is the distance between the nth relay and the destination. We simulated three different impulsive noise environments: near-Gaussian with $(\lambda,\Gamma) = (1, 0.1)$, highly impulsive with $(\lambda,\Gamma) = (10^{-2}, 0.1)$, and very highly impulsive with $(\lambda,\Gamma) = (10^{-3}, 0.1)$. We studied the performances of ML, IML, and MD detectors in terms of ABER and diversity order as a function of the SNR. As a reference, the ABER of the optimum detector for the classical Rayleigh-fading channel affected by AWGN with variance σ^2, which is referred to as "Gauss" in the plots, was additionally reported. For each of the 10^6 Monte Carlo runs carried out (wherein, in addition to the network configuration, channel coefficients, impulsive noise, data sequences, and randomization coefficients are randomly generated), an independent record of 10^2 symbols was considered to evaluate the ABER and the APEP to be used in (1).

Example 3—Finite-SNR Diversity Order Analysis of the IML and MD Detectors for Different STBC Rules: In this example, the left-side plot in Fig. 2 shows the comparison between the diversity order $G_d^{\mathrm{iml}}(\gamma)$ defined by (22), which was evaluated by using (1) and averaging the exact expression of $\mathrm{PEP}_{\mathrm{iml}}(\mathbf{h},\mathbf{m})$ reported in (10), and its expression given by (23). We resorted to the same simulation setting of Examples 1 and 2. It is confirmed that the result (23) of Theorem 2 is exact. Additionally, we reported in the right-side plot in Fig. 2 the comparison between the estimated diversity order $\widehat{G}_d^{\mathrm{md}}(\gamma)$ (see Theorem 4) and its exact counterpart $G_d^{\mathrm{md}}(\gamma)$ defined by (46), which was evaluated by using (1) and averaging the exact expression of $\mathrm{PEP}_{\mathrm{md}}(\mathbf{h},\mathbf{m})$ reported in (41). All the curves show good agreement between exact and approximate results for both the considered STBC rules, thus demonstrating that $\widehat{G}_d^{\mathrm{md}}(\gamma)$ is a good candidate for substituting $G_d^{\mathrm{md}}(\gamma)$ when theoretical findings are of concern.

Example 4—ABER Analysis With Alamouti STBC ($L = 2$): In this example, a QPSK signaling and the full-rate Alamouti code of order $L = K = P = 2$ [47] was used, as in Example 1. Figs. 3 and 4 refer to the case of $N_{\max} = 3$ potential relays for near-Gaussian and very highly impulsive noise, respectively. In this case, the asymptotic diversity order of all the schemes under comparison is equal to $R_{\max} = \min\{L, N_{\max}+1\} = 2$. In the left-side plot, the number of active relays in Phase II is kept fixed to 3, whereas in the right-side plot, the number of active relays in Phase II is randomly time varying according to the statistical distribution of vector $\tilde{\mathbf{s}}$ discussed in Section II. It is apparent from all the figures that the ABER curves of the IML detector strictly follow the corresponding curves of the ML detector. In particular, independently of the detecting structure employed at the destination, the complex Gaussian decentralized scheme only pays slight performance degradation with respect to its centralized counterpart in both noise environments. Moreover, with reference to the very highly impulsive noise case, the fluctuating trend of the finite-SNR diversity order of the MD detector significantly penalizes the ABER

$$\widehat{G}_d^{\mathrm{md}}(\gamma) \approx \min_{\substack{k,\ell\in\{1,2,\ldots,|\mathcal{A}|\}\\ \ell\neq k}} \frac{v_1(\gamma,\pi/2,0)v_2(\gamma,\pi/2,0) + \lambda v_1(\gamma,\pi/2,1)v_2(\gamma,\pi/2,1)}{v_1(\gamma,\pi/2,0) + \lambda v_1(\gamma,\pi/2,1)} \tag{51}$$

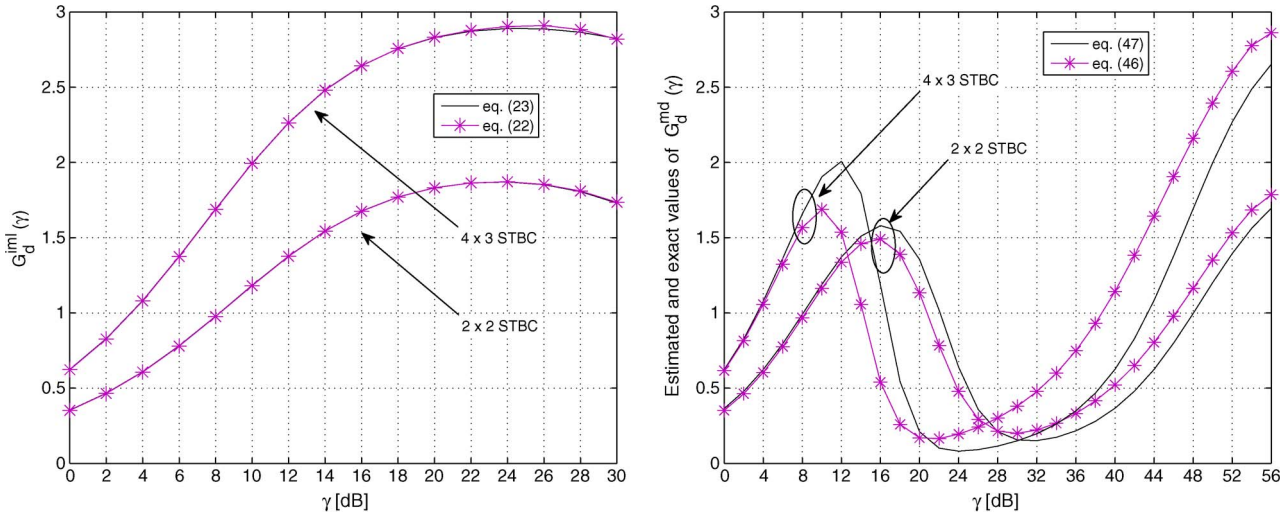

Fig. 2. Very highly impulsive noise. Comparison between (left-side plot) (22) and (23) and (right-side plot) (46) and (47) versus γ for different STBC rules (Example 3: QPSK signaling, $N_{\max} = L - 1$, $\lambda = 10^{-3}$, $\Gamma = 0.1$, and $\sigma_{g_0}^2 \triangleq 10^{-2}$).

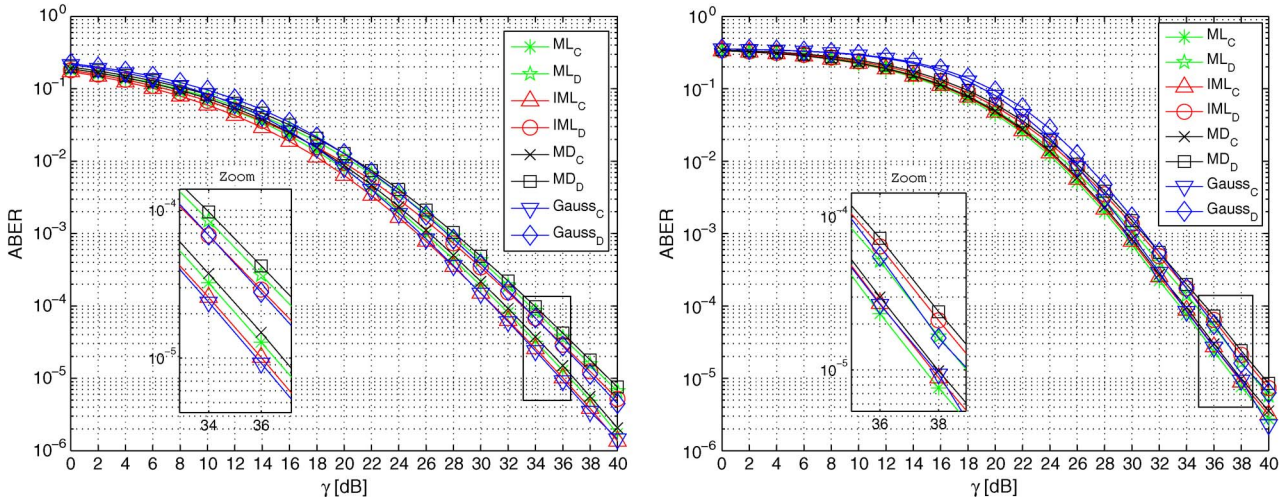

Fig. 3. Near-Gaussian noise. ABER versus SNR (Example 4: 2×2 Alamouti complex code and $N_{\max} = 3$ potential relays). (Left-side plot) The number of active relays in Phase II is fixed to 3. (Right-side plot) The number of active relays in Phase II is randomly time varying.

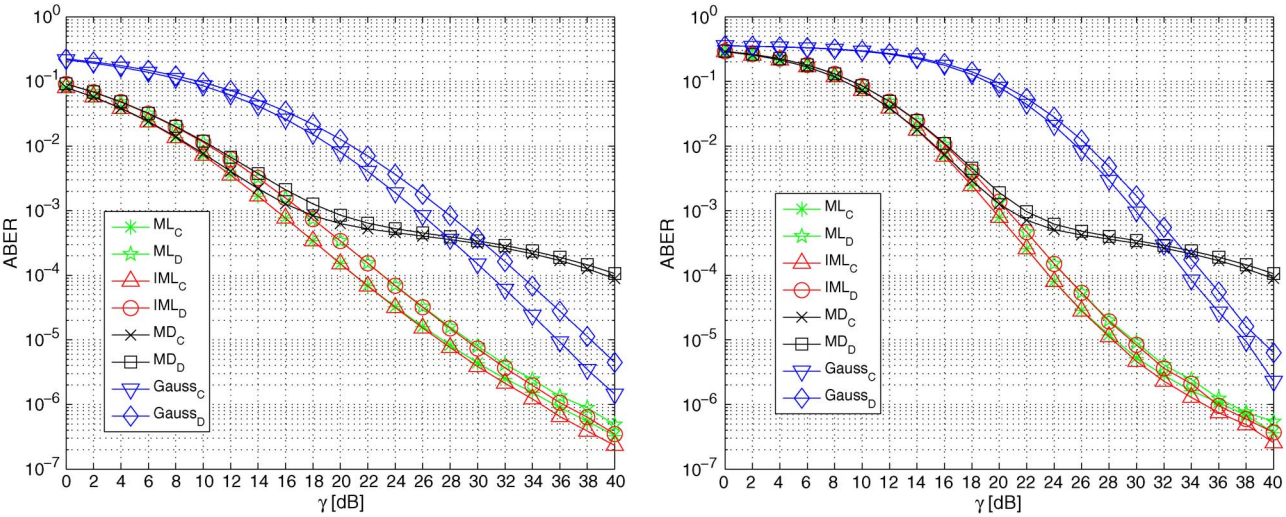

Fig. 4. Very highly impulsive noise. ABER versus SNR (Example 4: 2×2 Alamouti complex code and $N_{\max} = 3$ potential relays). (Left-side plot) The number of active relays in Phase II is fixed to 3. (Right-side plot) The number of active relays in Phase II is randomly time varying.

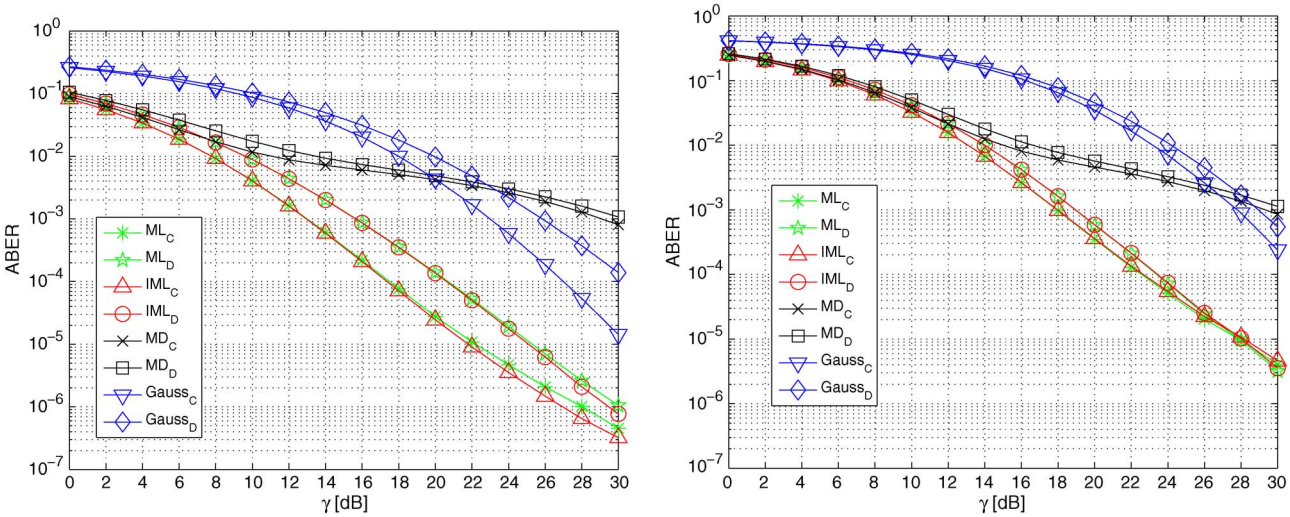

Fig. 5. Highly impulsive noise. ABER versus SNR (Example 5: 4×3 complex orthogonal code and $N_{\max} = 2$ potential relays). (Left-side plot) The number of active relays in Phase II is fixed to 2. (Right-side plot) The number of active relays in Phase II is randomly time varying.

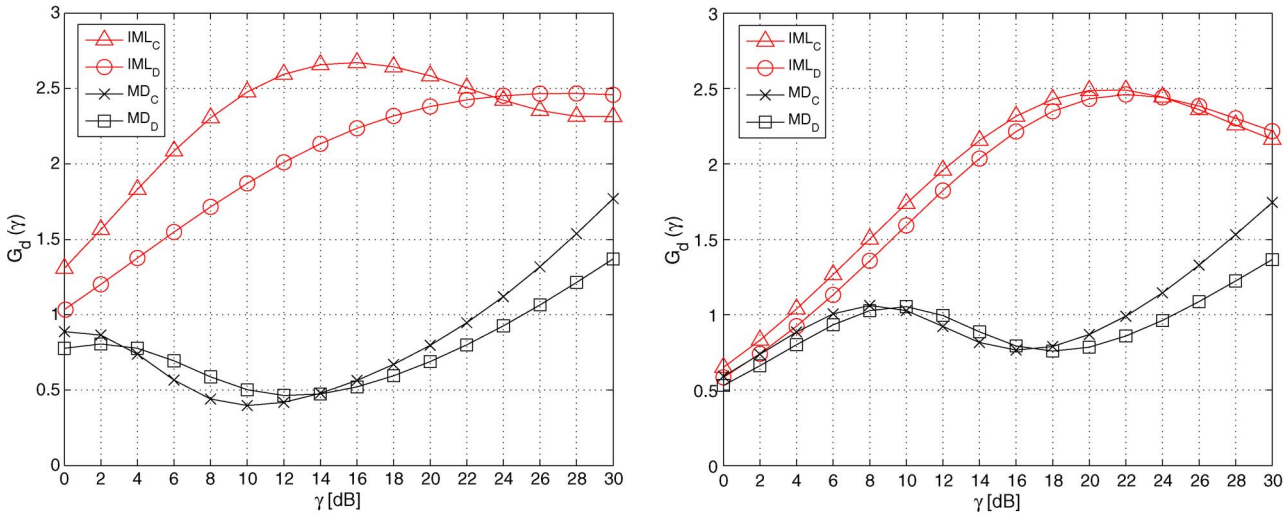

Fig. 6. Highly impulsive noise. Diversity order versus SNR (Example 5: 4×3 complex orthogonal code and $N_{\max} = 2$ potential relays). (Left-side plot) The number of active relays in Phase II is fixed to 2. (Right-side plot) The number of active relays in Phase II is randomly time varying.

performance of such a detector in both its centralized and decentralized versions. Results not reported here for the sake of brevity show that by increasing the number of potential relays, a slight performance gain can be achieved for all the schemes under comparison. Finally, the randomness in the number of active relays impacts both the coding gain and the diversity order of the detectors in both noise environments; in particular, it is worth noticing that for moderate-to-high SNR values, such an impact on the diversity order is not significant, i.e., each ABER curve in the left-side plots in Figs. 3 and 4 exhibits a similar slope to the corresponding curve in the right-side plots.

Example 5—ABER and Finite-SNR Diversity Order Analysis With Orthogonal STBC of Order $L = 3$: In this example, a BPSK signaling, i.e., $\tilde{a}_k = \{\pm 1\}$, for $k \in \{1, 2, \ldots, K\}$ was used, to reduce the implementation complexity of the ML detector. We considered as STBC rule the complex orthogonal code of order $L = K = 3$ with a code rate of $K/P = 3/4$ [48]. The ABER curves in Fig. 5 and the finite-SNR diversity order results in Fig. 6, the latter were obtained by using (1) and averaging (10) and (41), refer to the case of $N_{\max} = 2$ active relays for highly impulsive noise. In this case, the asymptotic diversity order of all the schemes under comparison is equal to $R_{\max} = \min\{L, N_{\max} + 1\} = 3$. In the left-side plot, the number of active relays in Phase II is kept fixed to 2, whereas in the right-side plot, the number of active relays in Phase II is randomly time varying according to the statistical distribution of $\tilde{\mathbf{s}}$ discussed in Section II. In addition to confirming the results of Example 4, it is also apparent in Fig. 5 that in the case of highly impulsive noise, the larger is the diversity order, the more evident is the performance penalty of the MD detector with respect to the ML and IML detectors in terms of coding gain. This is in accordance with the theoretical results derived in Sections III-B2 and IV-B2. Finally, it can be argued in Fig. 6 that for $\gamma > 16$ dB, the diversity order of the MD detector when the number of relays is randomly time varying approximatively exhibits the same behavior as the case in which the number of relays is fixed, whereas the randomness in the number of active relays tends to smooth the difference between the diversity order of the centralized and decentralized IML detectors.

VI. Conclusion

We studied the performance of DSTBC D&F relaying schemes in the presence of MCA noise, by considering both optimal and suboptimal detecting structures at the destination. Our analytical analysis and simulation results show that the principal adverse impact of highly impulsive noise on the system performance is to significantly slow down the rate of convergence of the diversity order to its asymptotic value $R_{\max} = \min(L, N_{\max}+1)$. This effect is much more evident for the MD detector, which additionally pays a significant performance penalty with respect to the ML and IML detectors in terms of coding gain. Future research issues consist in applying our general framework to different relaying strategies and suboptimal detectors with memoryless nonlinearity.

Appendix A
Proof of Theorem 1

Accounting for (10), using the result [53] that $\mathrm{E}[\exp(-\tilde{\mathbf{g}}^H \mathbf{A}\tilde{\mathbf{g}})] = \det^{-1}(\mathbf{I}_N + \mathbf{\Sigma}_{\tilde{\mathbf{g}}}\mathbf{A})$, for $\mathbf{A} \in \mathbb{C}^{(N_{\max}+1)\times(N_{\max}+1)}$, and remembering that $\det(\mathbf{I}_N + \mathbf{BC}) = \det(\mathbf{I}_P + \mathbf{CB})$, for $\mathbf{B} \in \mathbb{C}^{(N_{\max}+1)\times P}$ and $\mathbf{C} \in \mathbb{C}^{P\times(N_{\max}+1)}$, one has (56) shown at the bottom of the page, where $\gamma \triangleq 1/\sigma^2$ and $\mathbf{\Phi}_{k,\ell}(\mathbf{s}) \triangleq \mathcal{C}_{k,\ell}\mathcal{R}\mathbf{S}\mathbf{\Sigma}_{\tilde{\mathbf{g}}}\mathbf{S}\mathcal{R}^H\mathcal{C}_{k,\ell}^H \in \mathbb{C}^{P\times P}$ is a given matrix. Since the diagonal matrix $\mathbf{\Sigma}_{\tilde{\mathbf{g}}}$ is nonsingular and the rank of a matrix is unchanged upon left or right multiplication by a nonsingular matrix [50], it follows that $\mathrm{rank}(\mathbf{\Phi}_{k,\ell}(\mathbf{s})) = \mathrm{rank}(\mathcal{C}_{k,\ell}\mathcal{R}\mathbf{S})$. Moreover, since $\mathrm{rank}(\mathcal{C}_{k,\ell}) = \min(P, L)$ (rank criterion) and $R(\mathbf{s}) = \mathrm{rank}(\mathcal{R}\mathbf{S}) = \min(L, N(\mathbf{s})+1)$, it results [50] that $\min(P, L) + R(\mathbf{s}) - L \le \mathrm{rank}(\mathcal{C}_{k,\ell}\mathcal{R}\mathbf{S}) \le \min(\min(P, L), R(\mathbf{s}))$. Hence, in the case of $P \ge L$, one has $\mathrm{rank}(\mathcal{C}_{k,\ell}\mathcal{R}\mathbf{S}) = R(\mathbf{s})$, and consequently, because matrix $\mathbf{\Sigma}_{\mathbf{m}}$ is nonsingular, one obtains $\mathrm{rank}(\mathbf{\Sigma}_{\mathbf{m}}^{-1}\mathbf{\Phi}_{k,\ell}(\mathbf{s})) = \mathrm{rank}(\mathbf{\Phi}_{k,\ell}(\mathbf{s})) = R(\mathbf{s}) \le P$. Then, since $\mathbf{\Phi}_{k,\ell}(\mathbf{s})$ is a positive semidefinite Hermitian matrix, i.e., its eigenvalues are nonnegative real numbers, and the eigenvalues of the diagonal matrix $\mathbf{\Sigma}_{\mathbf{m}}$ are simply equal to its diagonal entries (which are positive and are assumed to be arranged in increasing order, i.e., $\sigma_{m_1}^2 \le \sigma_{m_2}^2 \le \cdots \le \sigma_{m_P}^2$), one gets (57) shown at the bottom of the page. Therefore, by substituting (57) in (56) and accounting for (4), one has

$$\begin{aligned}
&\mathrm{E}_{\widetilde{\mathbf{m}}\,|\tilde{\mathbf{s}}=\mathbf{s},\tilde{\mathcal{R}}=\mathcal{R}}\left\{\mathrm{E}_{\tilde{\mathbf{g}}|\,\widetilde{\mathbf{m}}\,,\tilde{\mathbf{s}}=\mathbf{s},\tilde{\mathcal{R}}=\mathcal{R}}\left[\mathrm{PEP}_{\mathrm{iml}}(\tilde{\mathbf{h}}, \tilde{\mathbf{m}})\right]\right\} \\
&\quad \le \frac{\Theta}{\gamma^{R(\mathbf{s})}}\left(\prod_{p=P-R(\mathbf{s})+1}^{P}\frac{\mathrm{E}[\tilde{m}_p]\lambda^{-1}+\Gamma}{1+\Gamma}\right) \\
&\qquad \cdot\left[\prod_{r=1}^{R(\mathbf{s})}\mu_r\left(\mathbf{\Phi}_{k,\ell}(\mathbf{s})\right)\right]^{-1} = \frac{\Theta}{\gamma^{R(\mathbf{s})}}\prod_{r=1}^{R(\mathbf{s})}\mu_r^{-1}\left(\mathbf{\Phi}_{k,\ell}(\mathbf{s})\right) \quad (58)
\end{aligned}$$

with $\Theta \triangleq (4^{R(\mathbf{s})}/\pi)\int_0^{\pi/2}(\sin^2\theta)^{R(\mathbf{s})}d\theta$, where we have also used the fact that the Poisson RVs $\widetilde{m}_1, \widetilde{m}_2, \ldots, \widetilde{m}_P$ are statistically independent and $\mathrm{E}[\tilde{m}_p] = \lambda$. Let $\mathcal{R}\mathbf{S}\mathbf{\Sigma}_{\tilde{\mathbf{g}}}\mathbf{S}\mathcal{R}^H = \mathbf{U}\mathbf{\Omega}\mathbf{U}^H$ be the economy-size eigenvalue decomposition of $\mathcal{R}\mathbf{S}\mathbf{\Sigma}_{\tilde{\mathbf{g}}}\mathbf{S}\mathcal{R}^H$, with $\mathbf{U} \in \mathbb{C}^{L\times R(\mathbf{s})}$ satisfying $\mathbf{U}^H\mathbf{U} = \mathbf{I}_{R(\mathbf{s})}$ and

$$\begin{aligned}
\mathbf{\Omega} = \mathrm{diag}\big[&\mu_1(\mathcal{R}\mathbf{S}\mathbf{\Sigma}_{\tilde{\mathbf{g}}}\mathbf{S}\mathcal{R}^H), \mu_2(\mathcal{R}\mathbf{S}\mathbf{\Sigma}_{\tilde{\mathbf{g}}}\mathbf{S}\mathcal{R}^H), \ldots, \\
&\mu_R(\mathcal{R}\mathbf{S}\mathbf{\Sigma}_{\tilde{\mathbf{g}}}\mathbf{S}\mathcal{R}^H)\big] \in \mathbb{R}^{R(\mathbf{s})\times R(\mathbf{s})} \quad (59)
\end{aligned}$$

one has $\mu_r(\mathbf{\Phi}_{k,\ell}(\mathbf{s})) = \mu_r(\mathcal{C}_{k,\ell}\mathbf{U}\mathbf{\Omega}\mathbf{U}^H\mathcal{C}_{k,\ell}^H) = \mu_r(\mathbf{\Omega}\mathbf{U}^H\mathcal{C}_{k,\ell}^H\mathcal{C}_{k,\ell}\mathbf{U})$, for $r \in \{1, 2, \ldots, R(\mathbf{s})\}$. Moreover, it can be shown (see, e.g., [54]) that

$$\begin{aligned}
\prod_{r=1}^{R(\mathbf{s})}\mu_r\left(\mathbf{\Phi}_{k,\ell}(\mathbf{s})\right) &= \prod_{r=1}^{R(\mathbf{s})}\mu_r\left(\mathbf{\Omega}\mathbf{U}^H\mathcal{C}_{k,\ell}^H\mathcal{C}_{k,\ell}\mathbf{U}\right) \\
&\ge \left[\prod_{r=1}^{R(\mathbf{s})}\mu_r(\mathcal{R}\mathbf{S}\mathbf{\Sigma}_{\tilde{\mathbf{g}}}\mathbf{S}\mathcal{R}^H)\right] \\
&\quad \cdot\left[\prod_{r=L-R(\mathbf{s})+1}^{L}\mu_r\left(\mathbf{U}^H\mathcal{C}_{k,\ell}^H\mathcal{C}_{k,\ell}\mathbf{U}\right)\right]
\end{aligned}$$

$$\begin{aligned}
\mathrm{E}_{\tilde{\mathbf{g}}|\,\widetilde{\mathbf{m}}=\mathbf{m},\tilde{\mathbf{s}}=\mathbf{s},\tilde{\mathcal{R}}=\mathcal{R}}\left[\mathrm{PEP}_{\mathrm{iml}}(\tilde{\mathbf{h}}, \tilde{\mathbf{m}})\right] &= \frac{1}{\pi}\int_0^{\pi/2} E_{\tilde{\mathbf{g}}|\,\widetilde{\mathbf{m}}=\mathbf{m},\tilde{\mathbf{s}}=\mathbf{s},\tilde{\mathcal{R}}=\mathcal{R}}\left[\exp\left(-\frac{\tilde{\mathbf{g}}^H\mathbf{S}\mathcal{R}^H\mathcal{C}_{k,\ell}^H\mathbf{\Sigma}_{\mathbf{m}}^{-1}\mathcal{C}_{k,\ell}\mathcal{R}\mathbf{S}\tilde{\mathbf{g}}}{4\sigma^2\sin^2\theta}\right)\right]d\theta \\
&= \frac{1}{\pi}\int_0^{\pi/2}\det^{-1}\left(\mathbf{I}_P + \gamma\frac{\mathbf{\Sigma}_{\mathbf{m}}^{-1}\mathbf{\Phi}_{k,\ell}(\mathbf{s})}{4\sin^2\theta}\right)d\theta \quad (56)
\end{aligned}$$

$$\begin{aligned}
\det\left(\mathbf{I}_P + \gamma\frac{\mathbf{\Sigma}_{\mathbf{m}}^{-1}\mathbf{\Phi}_{k,\ell}(\mathbf{s})}{4\sin^2\theta}\right) &= \prod_{r=1}^{P}\left[1 + \gamma\frac{\mu_r\left(\mathbf{\Sigma}_{\mathbf{m}}^{-1}\mathbf{\Phi}_{k,\ell}(\mathbf{s})\right)}{4\sin^2\theta}\right]\left(\frac{\gamma}{4\sin^2\theta}\right)^{R(\mathbf{s})}\prod_{r=1}^{R(\mathbf{s})}\mu_r\left(\mathbf{\Sigma}_{\mathbf{m}}^{-1}\mathbf{\Phi}_{k,\ell}(\mathbf{s})\right) \\
&\ge \left(\frac{\gamma}{4\sin^2\theta}\right)^{R(\mathbf{s})}\left(\prod_{p=P-R(\mathbf{s})+1}^{P}\frac{1}{\sigma_{m_p}^2}\right)\left[\prod_{r=1}^{R(\mathbf{s})}\mu_r\left(\mathbf{\Phi}_{k,\ell}(\mathbf{s})\right)\right] \quad (57)
\end{aligned}$$

$$\geq \left[\prod_{r=1}^{R(\mathbf{s})} \mu_r(\boldsymbol{\mathcal{R}}\mathbf{S}\boldsymbol{\Sigma}_{\tilde{\mathbf{g}}}\mathbf{S}\boldsymbol{\mathcal{R}}^H)\right] \cdot \left[\prod_{r=L-R(\mathbf{s})+1}^{L} \mu_r\left(\boldsymbol{\mathcal{C}}_{k,\ell}^H\boldsymbol{\mathcal{C}}_{k,\ell}\right)\right]. \quad (60)$$

Similarly, it can be seen that

$$\prod_{r=1}^{R(\mathbf{s})} \mu_r(\boldsymbol{\mathcal{R}}\mathbf{S}\boldsymbol{\Sigma}_{\tilde{\mathbf{g}}}\mathbf{S}\boldsymbol{\mathcal{R}}^H) = \prod_{r=1}^{R(\mathbf{s})} \mu_r(\boldsymbol{\Sigma}_{\tilde{\mathbf{g}}}\mathbf{S}\boldsymbol{\mathcal{R}}^H\boldsymbol{\mathcal{R}}\mathbf{S}) \geq \left[\prod_{r=N(\mathbf{s})-R(\mathbf{s})+1}^{N(\mathbf{s})} \sigma_{\tilde{g}_r}^2\right]\left[\prod_{r=1}^{R(\mathbf{s})} \mu_r(\mathbf{S}\boldsymbol{\mathcal{R}}^H\boldsymbol{\mathcal{R}}\mathbf{S})\right]. \quad (61)$$

Inequality (23) comes from substituting (60) and (61) in (58) and accounting for (11).

Appendix B
Proof of Lemma 1

Let us study the solution of (20). The eigenvalues $\mu_r(\boldsymbol{\mathcal{R}}^H\boldsymbol{\mathcal{R}})$ are necessarily positive for $r \in \{1, 2, \ldots, R_{\max}\}$, whereas $\mu_r(\boldsymbol{\mathcal{R}}^H\boldsymbol{\mathcal{R}}) = 0$ for $r \in \{R_{\max}+1, R_{\max}+2, \ldots, N_{\max}+1\}$. Thus, the application of the arithmetic–geometric mean inequality for nonnegative real numbers [50] leads to

$$\prod_{r=1}^{R_{\max}} \mu_r(\boldsymbol{\mathcal{R}}^H\boldsymbol{\mathcal{R}}) \leq \left[\frac{1}{R_{\max}}\sum_{r=1}^{R_{\max}} \mu_r(\boldsymbol{\mathcal{R}}^H\boldsymbol{\mathcal{R}})\right]^{R_{\max}} = \left[\frac{1}{R_{\max}}\text{trace}(\boldsymbol{\mathcal{R}}^H\boldsymbol{\mathcal{R}})\right]^{R_{\max}} = \left(\frac{\rho}{R_{\max}}\right)^{R_{\max}} \quad (62)$$

where we have also applied the constraint $\text{trace}(\boldsymbol{\mathcal{R}}^H\boldsymbol{\mathcal{R}}) = \rho$. In (62), equality holds if and only if

$$\mu_r(\boldsymbol{\mathcal{R}}^H\boldsymbol{\mathcal{R}}) = \frac{\rho}{R_{\max}} \quad \text{for } r \in \{1, 2, \ldots, R_{\max}\}. \quad (63)$$

When $L < N_{\max}+1$, i.e., $R_{\max} = L$, one has that $\mu_r(\boldsymbol{\mathcal{R}}^H\boldsymbol{\mathcal{R}}) = \mu_r(\boldsymbol{\mathcal{R}}\boldsymbol{\mathcal{R}}^H)$, for $r \in \{1, 2, \ldots, L\}$, and $\boldsymbol{\mathcal{R}}\boldsymbol{\mathcal{R}}^H$ is positive definite. In this case, condition (63) is fulfilled if and only if $\boldsymbol{\mathcal{R}}_{\text{opt}}\boldsymbol{\mathcal{R}}_{\text{opt}}^H = (\rho/L)\mathbf{I}_L$.

Let us now derive the solution of (21). The eigenvalues $\mu_r(\mathbf{S}\boldsymbol{\mathcal{R}}^H\boldsymbol{\mathcal{R}}\mathbf{S})$ are necessarily positive for $r \in \{1, 2, \ldots, R(\mathbf{s})\}$, whereas $\mu_r(\mathbf{S}\boldsymbol{\mathcal{R}}^H\boldsymbol{\mathcal{R}}\mathbf{S}) = 0$ for $r \in \{R(\mathbf{s})+1, R(\mathbf{s})+2, \ldots, N(\mathbf{s})+1\}$. Thus, applying again the arithmetic–geometric mean inequality, using the constraint $\text{trace}(\mathbf{S}\boldsymbol{\mathcal{R}}^H\boldsymbol{\mathcal{R}}\mathbf{S}) = \rho R(\mathbf{s})/R_{\max}$, and reasoning as previously done, one has that $\prod_{r=1}^{R(\mathbf{s})} \mu_r(\mathbf{S}\boldsymbol{\mathcal{R}}^H\boldsymbol{\mathcal{R}}\mathbf{S})$ is maximized when

$$\mu_r(\mathbf{S}\boldsymbol{\mathcal{R}}^H\boldsymbol{\mathcal{R}}\mathbf{S}) = \frac{\rho}{R_{\max}} \quad \text{for } r \in \{1, 2, \ldots, R(\mathbf{s})\} \quad (64)$$

and the corresponding maximum value is $(\rho/R_{\max})^{R(\mathbf{s})}$. Since $L \geq N_{\max}+1$, it follows that $R_{\max} = N_{\max}+1$ and $R(\mathbf{s}) = N(\mathbf{s})+1$. Let $\boldsymbol{\mathcal{R}}(\mathbf{s}) \in \mathbb{C}^{L\times(N(\mathbf{s})+1)}$ denote the matrix $\boldsymbol{\mathcal{R}}\mathbf{S}$ deprived of all its zero columns, then $\mu_r(\mathbf{S}\boldsymbol{\mathcal{R}}^H\boldsymbol{\mathcal{R}}\mathbf{S}) = \mu_r(\boldsymbol{\mathcal{R}}^H(\mathbf{s})\boldsymbol{\mathcal{R}}(\mathbf{s}))$. Consequently, $\boldsymbol{\mathcal{R}}^H(\mathbf{s})\boldsymbol{\mathcal{R}}(\mathbf{s})$ is positive definite, and hence, condition (64) is fulfilled for each realization $\mathbf{s}$ of $\tilde{\mathbf{s}}$ if and only if $\boldsymbol{\mathcal{R}}_{\text{opt}}^H\boldsymbol{\mathcal{R}}_{\text{opt}} = [\rho/(N_{\max}+1)]\mathbf{I}_{N_{\max}+1}$.

Appendix C
Proof of Theorem 2

Accounting for (56), using (4), and remembering that the Poisson RVs $\widetilde{m}_1, \widetilde{m}_2, \ldots, \widetilde{m}_P$ are statistically independent, one obtains

$$\begin{aligned}\text{APEP}(\gamma) &= \mathrm{E}_{\widetilde{\mathbf{m}}|\tilde{\mathbf{s}}=\mathbf{1}_{N_{\max}},\tilde{\boldsymbol{\mathcal{R}}}=\boldsymbol{\mathcal{R}}}\left\{\mathrm{E}_{\tilde{\mathbf{g}}|\,\widetilde{\mathbf{m}},\tilde{\mathbf{s}}=\mathbf{1}_{N_{\max}},\tilde{\boldsymbol{\mathcal{R}}}=\boldsymbol{\mathcal{R}}}\left[\text{PEP}_{\text{iml}}(\tilde{\mathbf{h}}, \tilde{\mathbf{m}})\right]\right\} \\ &= \frac{1}{\pi}\sum_{m_1=0}^{+\infty}\sum_{m_2=0}^{+\infty}\cdots\sum_{m_P=0}^{+\infty}\left[\prod_{p=1}^{P} p_{\widetilde{m}_p}(m_p)\right] \cdot \int_0^{\pi/2} \det{}^{-1}\left(\mathbf{I}_P + \gamma\frac{\boldsymbol{\Sigma}_{\mathbf{m}}^{-1}\boldsymbol{\Phi}_{k,\ell}}{4\sin^2\theta}\right) d\theta \end{aligned} \quad (65)$$

with $\boldsymbol{\Phi}_{k,\ell} \triangleq \boldsymbol{\Phi}_{k,\ell}(\mathbf{1}_{\max})$ (see Appendix A). It is convenient to observe that, by virtue of (4), one can write

$$\prod_{p=1}^{P} p_{\widetilde{m}_p}(m_p) = \exp(-\lambda P)\prod_{p=1}^{P}\frac{\lambda^{m_p}}{m_p!} = \exp(-\lambda P)\det(\boldsymbol{\Lambda}_{\mathbf{m}}) \quad (66)$$

where $\boldsymbol{\Lambda}_{\mathbf{m}} \triangleq \text{diag}(\lambda^{m_1}/m_1!, \lambda^{m_2}/m_2!, \ldots, \lambda^{m_P}/m_P!)$. According to (1), we have to evaluate the derivative of APEP(γ) with respect to the SNR. By invoking Leibnitz's rule, one gets

$$\frac{d\text{APEP}(\gamma)}{d\gamma} = \frac{\exp(-\lambda P)}{\pi}\sum_{m_1=0}^{+\infty}\sum_{m_2=0}^{+\infty}\cdots\sum_{m_P=0}^{+\infty}\det(\boldsymbol{\Lambda}_{\mathbf{m}}) \cdot \int_0^{\pi/2}\frac{\partial}{\partial\gamma}\det{}^{-1}\left(\mathbf{I}_P + \gamma\frac{\boldsymbol{\Sigma}_{\mathbf{m}}^{-1}\boldsymbol{\Phi}_{k,\ell}}{4\sin^2\theta}\right) d\theta \quad (67)$$

where by observing that

$$\frac{\partial\det(\mathbf{A})}{\partial\gamma} = \det(\mathbf{A})\text{trace}\left(\mathbf{A}^{-1}\frac{\partial\mathbf{A}}{\partial\gamma}\right)$$

where $\mathbf{A}$ is an arbitrary nonsingular square matrix depending on γ, it follows that

$$\begin{aligned}&\frac{\partial}{\partial\gamma}\det{}^{-1}\left(\mathbf{I}_P + \gamma\frac{\boldsymbol{\Sigma}_{\mathbf{m}}^{-1}\boldsymbol{\Phi}_{k,\ell}}{4\sin^2\theta}\right) \\ &\quad = -\det{}^{-1}\left(\mathbf{I}_P + \gamma\frac{\boldsymbol{\Sigma}_{\mathbf{m}}^{-1}\boldsymbol{\Phi}_{k,\ell}}{4\sin^2\theta}\right) \\ &\qquad \cdot\text{trace}\left[\left(\mathbf{I}_P + \gamma\frac{\boldsymbol{\Sigma}_{\mathbf{m}}^{-1}\boldsymbol{\Phi}_{k,\ell}}{4\sin^2\theta}\right)^{-1}\frac{\boldsymbol{\Sigma}_{\mathbf{m}}^{-1}\boldsymbol{\Phi}_{k,\ell}}{4\sin^2\theta}\right]. \end{aligned} \quad (68)$$

After simple rearrangements, (23) comes from substituting (65)–(68) in (1) and accounting for (22). The rank of the matrix $\boldsymbol{\Sigma}_{\mathbf{m}}^{-1}\boldsymbol{\Phi}_{k,\ell}$ can be obatined from the discussion in Appendix A.

APPENDIX D
PROOF OF THEOREM 3

Starting from (41) and reasoning as done for obtaining (56), one gets

$$\mathrm{E}_{\tilde{\mathbf{g}}|\,\widetilde{\mathbf{m}}=\mathbf{m},\tilde{\mathbf{s}}=\mathbf{s},\tilde{\boldsymbol{\mathcal{R}}}=\boldsymbol{\mathcal{R}}}\left[\mathrm{PEP}_{\mathrm{md}}(\tilde{\mathbf{h}},\tilde{\mathbf{m}})\right] \leq \frac{1}{\pi}\int_0^{\pi/2} E_{\tilde{\mathbf{g}}|\,\widetilde{\mathbf{m}}=\mathbf{m},\tilde{\mathbf{s}}=\mathbf{s},\tilde{\boldsymbol{\mathcal{R}}}=\boldsymbol{\mathcal{R}}}\left[\exp\left(-\frac{\tilde{\mathbf{g}}^H\mathbf{S}\boldsymbol{\mathcal{R}}^H\boldsymbol{\mathcal{C}}_{k,\ell}^H\boldsymbol{\mathcal{C}}_{k,\ell}\boldsymbol{\mathcal{R}}\mathbf{S}\tilde{\mathbf{g}}}{4\sigma^2\mu_1(\boldsymbol{\Sigma}_{\mathbf{m}})\sin^2\theta}\right)\right] d\theta$$
$$= \frac{1}{\pi}\int_0^{\pi/2}\det{}^{-1}\left[\mathbf{I}_P+\gamma\frac{\boldsymbol{\Phi}_{k,\ell}(\mathbf{s})}{4\mu_1(\boldsymbol{\Sigma}_{\mathbf{m}})\sin^2\theta}\right]d\theta \tag{69}$$

where γ and $\boldsymbol{\Phi}_{k,\ell}(\mathbf{s})$ have been defined in Appendix A. Using (69) and following the same steps that led to (57), one has

$$\mathrm{E}_{\tilde{\mathbf{g}}|\,\widetilde{\mathbf{m}}=\mathbf{m},\tilde{\mathbf{s}}=\mathbf{s},\tilde{\boldsymbol{\mathcal{R}}}=\boldsymbol{\mathcal{R}}}\left[\mathrm{PEP}_{\mathrm{md}}(\tilde{\mathbf{h}},\tilde{\mathbf{m}})\right] \leq [\mu_1(\boldsymbol{\Sigma}_{\mathbf{m}})]^{R(\mathbf{s})}\frac{\Theta}{\gamma^{R(\mathbf{s})}}\prod_{r=1}^{R(\mathbf{s})}\mu_r^{-1}\left(\boldsymbol{\Phi}_{k,\ell}(\mathbf{s})\right) \tag{70}$$

where Θ has been defined in Appendix A. Therefore, by observing that $\mu_1(\boldsymbol{\Sigma}_{\mathbf{m}})=\max(\sigma^2_{m_1},\sigma^2_{m_2},\ldots,\sigma^2_{m_P})$ and accounting for (4), one has

$$\mathrm{E}_{\tilde{\mathbf{g}}|\,\widetilde{\mathbf{m}}\,|\tilde{\mathbf{s}}=\mathbf{s},\tilde{\boldsymbol{\mathcal{R}}}=\boldsymbol{\mathcal{R}}}\left\{\mathrm{E}_{\tilde{\mathbf{g}}|\,\widetilde{\mathbf{m}}\,,\tilde{\mathbf{s}}=\mathbf{s},\tilde{\boldsymbol{\mathcal{R}}}=\boldsymbol{\mathcal{R}}},\left[\mathrm{PEP}_{\mathrm{md}}(\tilde{\mathbf{h}},\tilde{\mathbf{m}})\right]\right\}$$
$$\leq \mathrm{E}\left[\left(\frac{\tilde{m}\lambda^{-1}+\Gamma}{1+\Gamma}\right)^{R(\mathbf{s})}\right]\frac{\Theta}{\gamma^{R(\mathbf{s})}}\prod_{r=1}^{R(\mathbf{s})}\mu_r^{-1}\left(\boldsymbol{\Phi}_{k,\ell}(\mathbf{s})\right) \tag{71}$$

where $\tilde{m}\triangleq\max\{\tilde{m}_1,\tilde{m}_2,\ldots,\tilde{m}_P\}$. Since the maximum of P quantities is less than or equal to any number $m\in\mathbb{N}$ if and only if all of these quantities are less than or equal to m, and $\tilde{m}_1,\tilde{m}_2,\ldots,\tilde{m}_P$ are i.i.d. RVs, it follows that $P(\tilde{m}\leq m)=[F(m)]^P$ and $P(\tilde{m}\geq m)=1-[F(m-1)]^P$, where $F(m)\triangleq F_{\widetilde{m}_p}(m)=\sum_{i=0}^{m}p_{\widetilde{m}_p}(i)$ is the cumulative distribution function (cdf) of $\tilde{m}_p$, which does not depend on p. Consequently, one has

$$\begin{aligned}P(\tilde{m}=m)&=P\left(\{\tilde{m}\leq m\}\cap\{\tilde{m}\geq m\}\right)\\&=[F(m)]^P-[F(m-1)]^P\\&\leq P\left[F(m)-F(m-1)\right]=Pp_{\widetilde{m}_p}(m)\end{aligned} \tag{72}$$

where the inequality comes from Ruffini's rule and from the fact that the cdf of an RV is a positive number less than or equal to 1. Thus, one has

$$\mathrm{E}\left[\left(\frac{\tilde{m}\lambda^{-1}+\Gamma}{1+\Gamma}\right)^{R(\mathbf{s})}\right]=\sum_{m=0}^{+\infty}\left(\frac{m\lambda^{-1}+\Gamma}{1+\Gamma}\right)^{R(\mathbf{s})}P(\tilde{m}=m)$$
$$\leq P\mathrm{E}\left[\left(\frac{\widetilde{m}_p\lambda^{-1}+\Gamma}{1+\Gamma}\right)^{R(\mathbf{s})}\right]. \tag{73}$$

Inequality (42) comes from substituting (60), (61), and (73) in (71).

ACKNOWLEDGMENT

The authors would like to thank the anonymous reviewers for their constructive comments and suggestions, which helped improve the quality of the manuscript.

REFERENCES

[1] J. N. Laneman and G. W. Wornell, "Distributed space–time-coded protocols for exploiting cooperative diversity in wireless networks," *IEEE Trans. Inf. Theory*, vol. 49, no. 10, pp. 2415–2425, Oct. 2003.
[2] A. Sendonaris, E. Erkip, and B. Aazhang, "User cooperation diversity—Part I. System description," *IEEE Trans. Commun.*, vol. 51, no. 11, pp. 1927–1948, Nov. 2003.
[3] A. Sendonaris, E. Erkip, and B. Aazhang, "User cooperation diversity—Part II. Implementation aspects and performance analysis," *IEEE Trans. Commun.*, vol. 51, no. 11, pp. 1939–1948, Nov. 2003.
[4] J. N. Laneman, D. Tse, and G. W. Wornell, "Cooperative diversity in wireless networks: Efficient protocols and outage behavior," *IEEE Trans. Inf. Theory*, vol. 50, no. 12, pp. 3062–3080, Dec. 2004.
[5] S. Yiu, R. Schober, and L. Lampe, "Distributed space–time block coding," *IEEE Trans. Commun.*, vol. 54, no. 7, pp. 1195–1206, Jul. 2006.
[6] B. Sirkeci-Mergen and A. Scaglione, "Randomized space–time coding for distributed cooperative communication," *IEEE Trans. Signal Process.*, vol. 55, no. 10, pp. 5003–5017, Oct. 2007.
[7] M. Sharp, A. Scaglione, and B. Sirkeci-Mergen, "Randomized cooperation in asynchronous dispersive links," *IEEE Trans. Commun.*, vol. 57, no. 1, pp. 64–68, Jan. 2009.
[8] F. Verde and A. Scaglione, "Randomized space–time block coding for distributed amplify-and-forward cooperative relays," in *Proc. IEEE ICASSP*, Dallas, TX, USA, Mar. 2010, pp. 3030–3033.
[9] F. Verde and A. Scaglione, "Decentralized space–time block coding for two-way relay networks," in *Proc. 11th IEEE Workshop SPAWC*, Marrakech, Morocco, Jun. 2010, pp. 1–5.
[10] F. Verde, "Design of randomized space–time block codes for amplify-and-forward cooperative relaying," in *Proc. 5th ISCCSP*, Rome, Italy, May 2012, pp. 1–5.
[11] F. Verde, D. Darsena, and A. Scaglione, "Cooperative randomized MIMO-OFDM downlink for multicell networks: Design and analysis," *IEEE Trans. Signal Process.*, vol. 58, no. 1, pp. 384–402, Jan. 2010.
[12] F. Verde, T. Korakis, E. Erkip, and A. Scaglione, "A simple recruitment scheme of multiple nodes for cooperative MAC," *IEEE Trans. Commun.*, vol. 58, no. 9, pp. 2667–2682, Sep. 2010.
[13] S. Bagheri, F. Verde, D. Darsena, and A. Scaglione, "Randomized decode-and-forward strategies for two-way relay networks," *IEEE Trans. Wireless Commun.*, vol. 10, no. 12, pp. 4214–4225, Dec. 2011.
[14] P. Liu, C. Nie, T. Korakis, E. Erkip, S. Panwar, F. Verde, and A. Scaglione, "STiCMAC: A MAC protocol for robust space–time coding in cooperative wireless LANs," *IEEE Trans. Wireless Commun.*, vol. 11, no. 4, pp. 1358–1369, Apr. 2012.
[15] V. Tarokh, N. Seshadri, and A. Calderbank, "Space–time codes for high data rate wireless communication: Performance criterion and code construction," *IEEE Trans. Inf. Theory*, vol. 44, no. 2, pp. 744–765, Mar. 1998.
[16] V. Tarokh, H. Jafarkhani, and A. Calderbank, "Space–time block codes from orthogonal designs," *IEEE Trans. Inf. Theory*, vol. 45, no. 5, pp. 1456–1467, Jul. 1999.
[17] K. L. Blackard, T. S. Rappaport, and C. W. Bostian, "Measurements and models of radio frequency impulsive noise for indoor wireless communications," *IEEE J. Sel. Areas Commun.*, vol. 11, no. 7, pp. 991–1001, Sep. 1993.
[18] T. K. Blankenship and T. S. Rappaport, "Characteristics of impulsive noise in the 450-MHz band in hospitals and clinics," *IEEE Trans. Antennas Propag.*, vol. 46, no. 2, pp. 194–203, Feb. 1998.
[19] M. G. Sanchez, I. Cuinas, and A. V. Alejos, "Interference and impairments in radio communication systems due to industrial shot noise," in *Proc. IEEE Int. Symp. Ind. Electron.*, Vigo, Spain, Jun. 2007, pp. 1849–1854.
[20] Q. Shan, I. A. Glover, R. C. Atkinson, S. A. Bhatti, I. E. Portugues, P. J. Moore, R. Rutherford, M. de Fatima Queiroz Vieira, A. M. N. Lima, and B. A. de Souza, "Estimation of impulsive noise in an electricity substation," *IEEE Trans. Electromagn. Compat.*, vol. 53, no. 3, pp. 653–663, Aug. 2011.
[21] L. Lampe, R. Schober, and S. Yiu, "Distributed space–time coding for multihop transmission in power line communication networks," *IEEE J. Sel. Areas Commun.*, vol. 24, no. 7, pp. 1389–1400, Jul. 2006.

[22] M. Kuhn, S. Berger, I. Hammerström, and A. Wittneben, "Power line enhanced cooperative wireless communications," *IEEE J. Sel. Areas Commun.*, vol. 24, no. 7, pp. 1401–1410, Jul. 2006.
[23] D. Middleton, "Statistical-physical models of electromagnetic interference," *IEEE Trans. Electromagn. Compat.*, vol. EMC-19, no. 3, pp. 106–127, Aug. 1977.
[24] A. D. Spaulding and D. Middleton, "Optimum reception in the impulse interference environment—Part I: Coherent detection," *IEEE Trans. Commun.*, vol. COM-25, no. 9, pp. 910–923, Sep. 1977.
[25] D. Middleton, "Procedure for determining the parameters of a first-order canonical models of class A and class B electromagnetic interference," *IEEE Trans. Electromagn. Compat.*, vol. EMC-21, no. 3, pp. 190–208, Aug. 1979.
[26] M. Ghosh, "Analysis of the effect of impulse noise on multicarrier and single-carrier QAM systems," *IEEE Trans. Commun.*, vol. 44, no. 2, pp. 145–147, Feb. 1996.
[27] J. Ilow and D. Hatzinakos, "Analytic alpha-stable noise modeling in a Poisson field of interferers or scatterers," *IEEE Trans. Signal Process.*, vol. 51, no. 1, pp. 64–76, Jan. 2003.
[28] C. Tepedelenliolu and P. Gao, "On the diversity reception over fading channels with impulsive noise," *IEEE Trans. Veh. Technol.*, vol. 54, no. 6, pp. 2037–2047, Nov. 2005.
[29] P. Gao and C. Tepedelenliolu, "Space–time coding over fading channels with impulsive noise," *IEEE Trans. Wireless Commun.*, vol. 6, no. 1, pp. 220–229, Jan. 2007.
[30] J. Lee and C. Tepedelenliolu, "Space–time coding over fading channels with stable noise," *IEEE Trans. Veh. Technol.*, vol. 60, no. 7, pp. 3169–3177, Sep. 2011.
[31] A. Nasri, R. Schober, and I. F. Blake, "Performance and optimization of amplify-and-forward cooperative diversity systems in generic noise and interference," *IEEE Trans. Wireless Commun.*, vol. 10, no. 4, pp. 1132–1143, Apr. 2011.
[32] H. Van Khuong and T. Le-Ngoc, "Effect of impulsive noise on decode-and-forward cooperative relaying over fading channel," in *Proc. IEEE WCNC*, Cancun, Mexico, Mar. 2011, pp. 1392–1397.
[33] S. Al-Dharrab and M. Uysal, "Cooperative diversity in the presence of impulsive noise," *IEEE Trans. Wireless Commun.*, vol. 8, no. 9, pp. 4730–4739, Sep. 2009.
[34] R. Savoia and F. Verde, "Performance analysis of decode-and-forward relaying in impulsive noise environments," in *Proc. 8th ISWCS*, Aachen, Germany, Nov. 2011, pp. 412–416.
[35] P. J. Huber, *Robust Statistics*. New York, USA: Wiley, 1981.
[36] X. Wang and H. V. Poor, "Robust multiuser detection in non-Gaussian channels," *IEEE Trans. Signal Process.*, vol. 47, no. 2, pp. 289–305, Feb. 1999.
[37] S. V. Zhidkov, "Analysis and comparison of several simple impulsive noise mitigation schemes for OFDM receivers," *IEEE Trans. Commun.*, vol. 56, no. 1, pp. 5–9, Jan. 2008.
[38] D. Tse and P. Viswanath, *Fundamentals of Wireless Communication*. Cambridge, U.K.: Cambridge Univ. Press, 2005.
[39] R. Narasimhan, "Finite-SNR diversity-multiplexing tradeoff for correlated Rayleigh and Rician MIMO channels," *IEEE Trans. Inf. Theory*, vol. 52, no. 9, pp. 3965–3979, Sep. 2006.
[40] P. A. Delaney, "Signal detection in multivariate class-A interference," *IEEE Trans. Commun.*, vol. 43, no. 2–4, pp. 365–373, Feb.–Apr. 1995.
[41] K. G. Seddik, A. K. Sadek, A. S. Ibrahim, and K. J. R. Liu, "Design criteria and performance analysis for distributed space–time coding," *IEEE Trans. Veh. Technol.*, vol. 57, no. 4, pp. 2280–2292, Jul. 2008.
[42] J. Häring and A. J. H. Vinck, "Performance bounds for optimum and suboptimum reception under Class-A impulsive noise," *IEEE Trans. Commun.*, vol. 50, no. 7, pp. 1130–1136, Jul. 2002.
[43] J. G. Proakis, *Digital Communications*. New York, NY, USA: McGraw-Hill, 2001.
[44] R. S. Blum, R. J. Kozick, and B. M. Sadler, "An adaptive spatial diversity receiver for non-Gaussian interference and noise," *IEEE Trans. Signal Process.*, vol. 47, no. 8, pp. 2100–2111, Aug. 1999.
[45] K. S. Vastola, "Threshold detection in narrow-band non-Gaussian noise," *IEEE Trans. Commun.*, vol. COM-32, no. 2, pp. 134–139, Feb. 1984.
[46] L. C. Tran, T. A. Wisocki, J. Seberry, A. Mertins, and S. S. Adams, "Novel constructions of improved square complex orthogonal designs for eight transmit antennas," *IEEE Trans. Inf. Theory*, vol. 55, no. 10, pp. 4439–4448, Oct. 2009.
[47] S. M. Alamouti, "A simple transmit diversity technique for wireless communications," *IEEE J. Sel. Areas Commun.*, vol. 16, no. 8, pp. 1451–1458, Oct. 1998.
[48] W. Su, X.-G. Xia, and K. J. R. Liu, "A systematic design of high-rate complex orthogonal space–time block codes," *IEEE Commun. Lett.*, vol. 8, no. 6, pp. 380–382, Jun. 2004.
[49] H. Jafarkhani, *Space–Time Coding—Theory and Practice*. Cambridge, U.K.: Cambridge Univ. Press, 2005.
[50] R. A. Horn and C. R. Johnson, *Matrix Analysis*. Cambridge, U.K.: Cambridge Univ. Press, 1990.
[51] A. Ben-Israel and T. N. E. Greville, *Generalized Inverses*. New York, NY, USA: Springer-Verlag, 2002.
[52] A. Papoulis, *Probability, Random Variables, and Stochastics Processes*, 3rd ed. Singapore: McGraw-Hill, 1991.
[53] N. R. Goodman, "Statistical analysis based on a certain multivariate complex Gaussian distribution (An introduction)," *Ann. Math. Stat.*, vol. 34, no. 1, pp. 152–177, Mar. 1963.
[54] A. W. Marshall and I. Olkin, *Inequalities: Theory of Majorization and Its Applications*. New York, NY, USA: Academic, 1979.

Roberto Savoia was born in Naples, Italy, on May 25, 1985. He received the Dr.Eng. degree (*summa cum laude*) in telecommunications engineering from the University of Naples Federico II, in 2010, where he is currently working toward the Ph.D. degree in electronic and telecommunications engineering with the Department of Electrical Engineering and Information Technology.

His research activities lie in the area of wireless communications. In particular, his current interests include cooperative and cognitive radio networks.

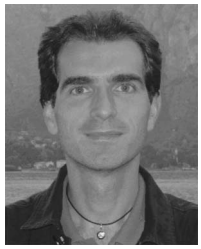

Francesco Verde (M'10) was born in Santa Maria Capua Vetere, Italy, on June 12, 1974. He received the Dr.Eng. degree (*summa cum laude*) in electronic engineering from the Second University of Naples, Naples, Italy, in 1998 and the Ph.D. degree in information engineering from the University of Naples Federico II, in 2002.

Since December 2002, he has been with the Department of Biomedical, Electronic, and Telecommunication Engineering, which, since January 2013, has been consolidated into the Department of Electrical Engineering and Information Technology, University of Naples Federico II. He first served as an Assistant Professor of signal theory and mobile communications and, since December 2011, has served as an Associate Professor of telecommunications. He has also held teaching positions at the Second University of Naples. His research activities lie in the broad area of statistical signal processing, digital communications, and communication systems. In particular, his current interests include cyclostationarity-based techniques for blind identification, equalization and interference suppression for narrowband modulation systems, code-division multiple-access systems, multicarrier modulation systems, space–time processing for cooperative and cognitive communications systems, and software-defined networks.

Prof. Verde has served as an Associate Editor for the IEEE TRANSACTIONS ON SIGNAL PROCESSING since September 2010.